25

Hydrogen Storage in Hollow Microspheres

Laurent Pilon
University of California, Los Angeles

CONTENTS

25.1 Introduction 764
25.1.1 Hydrogen Storage Technologies 764
25.1.2 Hydrogen Storage in Hollow Glass Microspheres 765
25.2 Design Parameters for Hydrogen Storage in Hollow Microspheres 769
25.2.1 Principles 769
25.2.2 Hydrogen Properties 769
25.2.2.1 Density 769
25.2.2.2 Compressibility Factor 771
25.2.3 Burst Pressure 771
25.2.4 Buckling Pressure 773
25.2.5 Hydrogen Permeation Processes 773
25.2.6 Geometric Considerations 774
25.2.7 Material Considerations 775
25.2.7.1 Mechanical and Thermal Properties 776
25.2.7.2 Hydrogen Permeability 776
25.2.7.3 Hydrogen Diffusion Coefficient and Solubility in Glass 779
25.2.7.4 Optical Properties 780
25.3 Performance Assessment 781
25.3.1 Gravimetric and Volumetric Energy Densities 781
25.3.2 Loading and Unloading Times 784
25.3.3 Filling and Discharging Energy Requirements 786
25.4 Experiments 789
25.5 Synthesis of Hollow Glass Microspheres 791
25.5.1 Hollow Microspheres in Fly Ash 791
25.5.2 Spray Pyrolysis Process 791
25.5.2.1 Blowing Process 792
25.5.2.2 Semiproduct Production 792
25.5.3 Liquid-Droplet Method 794
25.5.4 Hollow Glass Microspheres by Solgel Process 795
25.5.5 Hollow Silica Aerogel Spheres 795
25.5.6 Porous Wall Glass Hollow Microspheres 796
25.5.7 Surface Treatment and Additional Functionality 797
25.5.8 Other Materials and Shapes 798
25.6 Conclusions and Perspectives 799
Nomenclature 800
References 801

Downloaded by [Laurent Pilon] at 06:37 11 August 2014

25.1 Introduction

The element hydrogen is the most commonly found element in the universe. However, hydrogen molecules (H_2) are not readily available. As such, it is an energy carrier as opposed to a fuel. It can be used in various mobile applications such as (1) in proton exchange membrane (PEM) fuel cell for transportation systems or mobile devices (e.g., laptops and cell phones) where it catalytically reacts with oxygen to produce water and electricity, (2) in internal combustion engines for surface transportation where it can be mixed with liquid fuel [1,2], or (3) in rocket propulsion [3]. Akunets et al. [2] also suggested using a mixture of liquid oxygen and hydrogen in polymer microballoons for jet engine fuel [2].

Hydrogen storage for such mobile applications is arguably one of the main technological challenges for a viable hydrogen economy. This chapter focuses on hydrogen storage in hollow glass microspheres or microcapsules in general. First, various power sources and fuels for mobile applications are compared based on their energy densities. Then, competing hydrogen storage technologies are reviewed. Moreover, principles, design parameters, material considerations, and performances associated with hydrogen storage in hollow glass microspheres are discussed in detail. Processes for synthesizing hollow glass microspheres are also reviewed.

25.1.1 Hydrogen Storage Technologies

In order to compare different fuels and energy carriers as well as hydrogen storage solutions, it is useful to remember that (1) energy contained in 1 kg of hydrogen is equivalent to that in 1 gal (3.78 L) of gasoline and that (2) current gasoline or diesel tanks contain between 10 and 30 gal. However, fuel cells are more efficient than internal combustion engines, thus reducing the required amount of hydrogen on board to 5–8 kg. In addition, a midsize fuel cell car cruising at 100 km/h (62 mph) consumes about 400 mg of H_2/s, which needs to be delivered on demand [4].

The US Department of Energy (DOE) has developed a technology roadmap for hydrogen storage. It sets quantitative targets that would ensure vehicle autonomy greater than 300 miles as well as safe and flexible driving, fast refueling time, procedure, and retail sales comparable to existing ones [5]. The technical criteria for selecting a specific hydrogen storage technology for transportation applications and the associated 2015 US DOE targets have been identified as follows [5]:

1. *Safe operation under all circumstances* including road accidents since hydrogen reacts explosively with oxygen above the ignition temperature of 450°C at atmospheric pressure
2. *Large gravimetric energy density* defined as the mass of H_2 (or energy) stored per unit mass of storage systems, which should be larger than 9 wt.% or 10.8 MJ/kg
3. *Large volumetric energy density* defined as the mass of H_2 or energy stored per unit volume of storage systems, which should be larger 81 g of H_2/L or 9.72 MJ/L
4. *Refueling time* of hydrogen tanks as short as refueling with current fuels such as diesel or gasoline (2.5 min for 5 kg of H_2)
5. *Reversibility of uptake and release* so that the storage system can be used numerous times (1500 cycles from 1/4 to full) for reliability and cost-effectiveness

6. On-demand availability with a minimum mass flow rate of 0.02 g/s/kW
7. Operating temperatures between −40°C and 60°C to work in any weather conditions
8. *Low energy requirements* for loading and unloading H_2 in order to achieve maximum energy efficiency
9. *Safe dormancy properties*, that is, at room temperature, very little hydrogen should leak out from the storage solution making the storage safe while not in use for extended periods of time
10. Low fabrication and operation costs for a pretax cost of $2/kW/h

Gaseous hydrogen at room temperature without its storage tank has gravimetric energy density of 143 MJ/kg and therefore exceeds by far DOE's target. Unfortunately, gaseous hydrogen at standard temperature and pressure has volumetric energy density of 0.01079 MJ/L. Such a very low value requires that hydrogen be compressed drastically. Numerous techniques have been proposed and can be grouped as (1) compressed hydrogen gas, (2) liquid hydrogen, (3) cryoadsorption, and (4) [6–8]. High-pressure H_2 storage solutions at room temperature include gas cylinders, underground reservoirs, and hollow glass microspheres [9–11]. Hydrogen can also be stored in liquid phase at cryogenic temperatures (≤20 K). Low-temperature cryoadsorption of hydrogen is achieved in (1) carbon nanotubes [12], (2) activated carbon [13], (3) carbon aerogels [13], (4) metal-organic framework [14], and (5) zeolite. Chemical hydrogen storage includes (1) metal hydrides [8,15], (2) liquid (organic) hydrides, and (3) ammonia and methanol. Unfortunately, none of the current technologies meet the aforementioned 2015 performance and cost targets set by the US DOE by a wide margin [16,17].

As an energy carrier for transportation systems and portable applications, hydrogen storage performances should be compared with other fuels or power systems including (1) liquid fuels (e.g., gasoline, diesel, biodiesel, ethanol, and methanol), (2) batteries (e.g., lithium ion, fluoride ions, and zinc–air) used in hybrid and all-electric cars, (3) solid fuel (e.g., Al, Zn, and Li) used in rocket propulsion, (4) compressed or liquified natural gas already widely used for public transportation, and (5) compressed air. To do so, it is useful to define the gravimetric and volumetric energy densities representing the amount of energy stored in a system per unit mass or unit volume, respectively. Figure 25.1 plots the gravimetric versus volumetric energy densities for each fuel or energy storage technologies and the associated container as reported in the literature [11,18]. It is evident that gasoline or diesel or biodiesel has outstanding performances that explain their widespread use. These performances are only matched by those of solid fuels, which cannot be considered for surface transportation. Performances of battery technologies, however, remain an order of magnitude smaller than liquid fuels.

Figure 25.2 also compares the best reported performances of the various hydrogen storage technologies [8,11]. It is evident that metal hydrides offer large volumetric energy density but relatively low gravimetric density. Liquid H_2 storage at 20 K and atmospheric pressure as well as cryoadsorption and cryocompressed storages show good performance but require large energy for liquefaction (27.9% of the stored energy [8]). They also feature poor dormancy properties.

25.1.2 Hydrogen Storage in Hollow Glass Microspheres

As previously discussed, the volumetric energy density of gaseous hydrogen at room temperature is very small and falls short of the DOE targets [5]. One strategy to increase its

Downloaded by [Laurent Pilon] at 06:37 11 August 2014

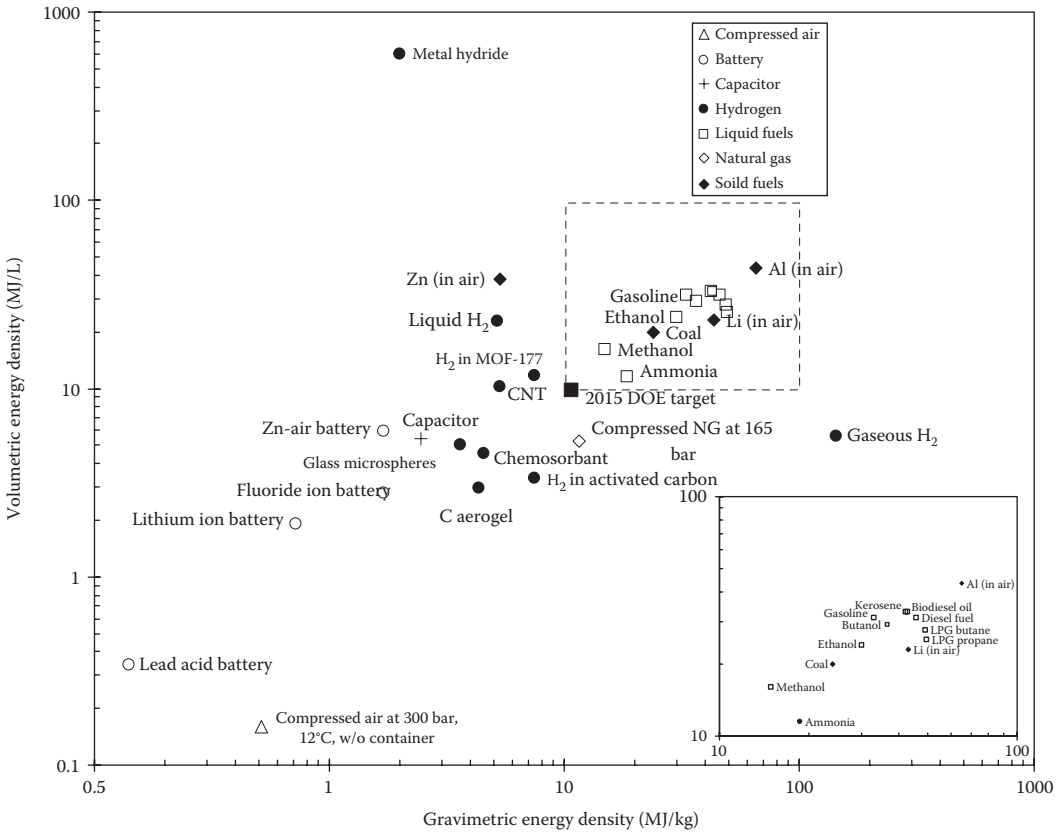

FIGURE 25.1
Comparison of gravimetric and volumetric energy densities for different fuels and hydrogen storage technologies. (From Yartys, V.A. and Lototsky, M.V., An overview of hydrogen storage methods, in *Hydrogen Materials Science and Chemistry of Carbon Nanomaterials*, Veziroglu, T.N., Zaginaichenko, S.Y., Schur, D.V., Baranowski, B., Shpak, A.P., Skorokhod, V.V., and Kale, A., eds., Kluwer Academic Publishers, Dordrecht, the Netherlands; Herr, M. and Lercher, J.A., Hydrogen storage in microspheres—Final report, ET-TN-03-628, September 9, 2003; Teitel, R.J., Microcavity hydrogen storage final progress report, Prepared for US Department of Energy and Environment, Report BNL 51439, 1981.)

volumetric energy density is to compress H_2 inside hollow glass microspheres or microcapsules in general. Loading and unloading of hydrogen gas in and out is based on the fact that gas permeation through the solid shell is a thermally activated process, that is, gas permeation increases exponentially with temperature. Hollow microspheres are also called microcapsules, microcavities, microbubbles, or microballoons. This was first proposed by Teitel in 1980 [9,10]. The initial thought was to use it in combination with a metal hydride storage system designed to store hydrogen released by hollow glass microspheres during cooldown and able to provide hydrogen during cold starts and accelerations. Moreover, "the addition of a metal hydride to the system would increase its hydrogen volumetric energy density and reduce the gravimetric energy density" [9]. Since then, hollow glass microspheres have been considered as stand-alone H_2 storage solutions [19]. Geometries other than microspheres have also been considered including microcylinders [4,20] and foams [21].

Figure 25.3 illustrates the typical life cycle of hollow microspheres for H_2 storage including (1) hydrogen loading, (2) storage and distribution, (3) onboard H_2 unloading,

Downloaded by [Laurent Pilon] at 06:37 11 August 2014

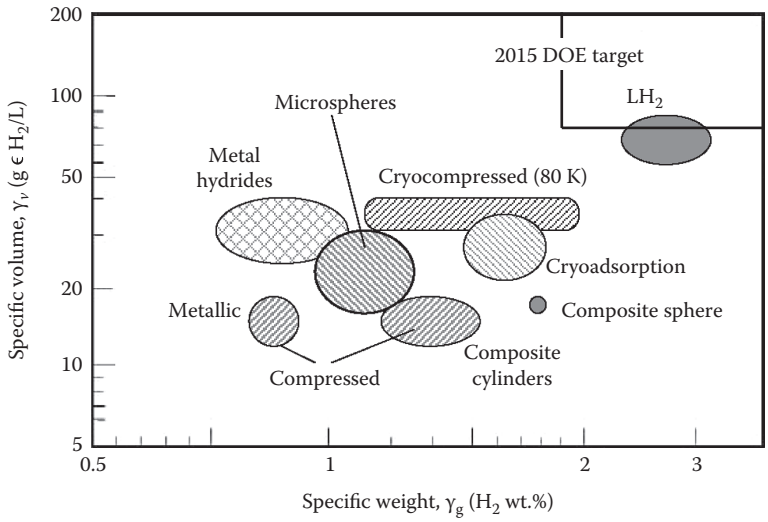

FIGURE 25.2
Comparison of gravimetric and volumetric energy densities for hydrogen storage technologies. (From Herr, M. and Lercher, J.A., Hydrogen storage in microspheres—Final report, ET-TN-03-628, September 9, 2003.)

Downloaded by [Laurent Pilon] at 06:37 11 August 2014

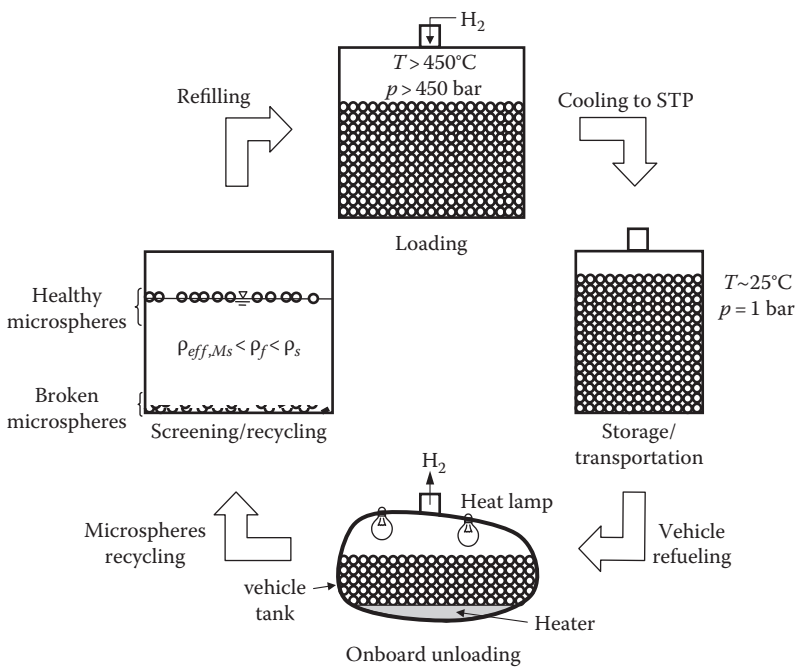

FIGURE 25.3
Life cycle of hollow microspheres from hydrogen loading and microsphere storage to vehicle refueling and microsphere recycling.

and (4) screening and recycling of healthy microcapsules. Practically, hydrogen loading in hollow microspheres can be performed at industrial scale in a batch process off vehicle in an autoclave at high temperatures (≈400°C) and pressures (>450 bar) to accelerate hydrogen permeation through the container's shell. Then, the hollow microspheres are cooled to room temperature so that hydrogen gas remains trapped inside due to significant reduction in the H_2 permeation with decreasing temperature (see Section 25.2.7.2). The hollow microspheres, then, can be safely transported to distribution points at room temperature and atmospheric pressure. Hydrogen refueling of a vehicle would consist of sucking the spent microspheres out of the tank and pouring loaded ones in the tank in a manner very similar to current gasoline or diesel refueling. On-demand hydrogen release from the microspheres would be induced by an onboard electric heater or a heat lamp integrated in the tank. Alternatively, unloading could also be achieved by mechanically or thermally destroying the microspheres, thus releasing their H_2 content. This strategy would still require removing the broken microspheres before tank refueling to be remelted or discarded. However, small pieces of broken microspheres could constitute a health hazard [22]. Empty microspheres removed from the tank would be screened for cracks and sorted by size and recycled to undergo the same sequence of H_2 loading, distribution, and unloading. Separation of broken microspheres from reusable ones can be achieved by the sink–float method [23,24]. This consists of placing all microspheres in a fluid whose density ρ_f is smaller than that of the shell materials ρ_s but larger than the effective density of the microspheres ρ_{MS}, that is, $\rho_{MS} < \rho_f < \rho_s$. Thus, pieces of broken microspheres will sink while *healthy* microspheres will float.

Hydrogen storage in hollow glass microspheres presents the following advantages over the previously reviewed storage technologies. First, hollow microspheres have high gravimetric energy density [11]. Hydrogen can be stored under internal pressure higher than that inside conventional cylinders [11]. Hydrogen-filled hollow glass microspheres are also easy and safe to handle at atmospheric pressure and ambient temperature and can be poured or pumped in tanks of any arbitrary geometries and made of lightweight materials (e.g., plastic) [11,19]. The technology is inexpensive and requires low energy consumption for producing large quantities of microcontainers [7]. In addition, this technology has good dormancy characteristics [7]. It is also resistant to contamination by atmospheric gases, unlike metal hydrides. Similarly, the microspheres are expected to remain stable and intrinsically safe under accident or fire conditions thanks to the small volume of hydrogen stored in each microspheres and their conformation or ability of the bed to change shape caused by potential deformation of the outside container [7,19,25]. Finally, the technical risks are minimal [7] and scaling from benchtop to full-scale utilization appears to be straightforward as hollow microspheres are already produced at industrial scale albeit for other applications and without the desired mechanical properties required for H_2 storage [26,27].

The challenges of hydrogen storage in microcontainers are [11,28] (1) the low volumetric energy density, (2) the relatively low fraction of recoverable hydrogen [29], (3) the fact that one needs to heat the microcapsules at temperatures above the operating temperature of PEM fuel cells, (4) the small H_2 release rate, (5) the large amount of energy required to compress hydrogen to very high pressures used during H_2 loading (25% of storage energy [8]), and (6) the cost of disposing or recycling glass microspheres. Table 25.1 summarizes the different advantages and disadvantages of hydrogen storage in microcapsules.

Downloaded by [Laurent Pilon] at 06:37 11 August 2014

TABLE 25.1

Established and Potential Advantages and Disadvantages Associated with Current Hydrogen Storage in Hollow Microcapsules

Advantages	Disadvantages
High gravimetric energy density	Low volumetric energy density
Handling at room temperature and atmospheric pressure	Requires hydrogen loading under very high pressures
Inexpensive and high-throughput manufacturing process	Requires heating for loading or unloading
Intrinsically safe	Potentially high loading energy cost
Good dormancy characteristics	Requires reprocessing of spent microcapsules
Resistant to contamination/poisoning by atmospheric gases	Potential health hazard from broken microcapsules
Can be poured and fit in any container solution	Uncertain consumer acceptance of refueling conditions
Easily scalable from lab to industrial scale	Large uncertainty in achieving desired performances
Minor technical risks	

Source: Robinson, S.L. and Handrock, J.L., Hydrogen storage for vehicular applications: Technology status and key development areas, Sandia National Laboratory Report SAND94-8229-UC-406, 1994.

Downloaded by [Laurent Pilon] at 06:37 11 August 2014

25.2 Design Parameters for Hydrogen Storage in Hollow Microspheres

25.2.1 Principles

The amount of hydrogen gas stored inside a capsule and its permeation rate depends on the inner and outer pressures, the temperature, and the shell material and thickness. To achieve the maximum storage capacity, pressure inside the microcapsules should be as large as possible. Similarly, for fast H_2 release, the outside pressure should be reduced and the temperature increased while the shell should be as thin as possible. However, the operating temperatures and pressures during loading and unloading and the handling of the hollow microcontainers should not threaten their mechanical integrity. The shell material should have the proper permeation properties but also the mechanical properties able to stand large pressures and temperatures as well as the thermal cycling associated with successive loading and unloading. Consequently, microcapsules' geometry and material as well as the operating temperatures and pressures must be optimized to minimize the loading and unloading times and to maximize the energy densities, the permeation rate, the hold time, and the number of life cycles. To do so, concepts of burst and buckling pressures, gas permeation, as well as geometric and material considerations are reviewed.

25.2.2 Hydrogen Properties

25.2.2.1 Density

At temperatures and pressures of interest for hydrogen storage, gaseous hydrogen cannot be considered as an ideal gas. Instead, a more complex equation of state must be used to

account for repulsion forces between H_2 molecules. The Beattie–Bridgeman equation gives the hydrogen pressure P as a function of temperature T and density ρ [30]:

$$P = \rho^2 RT\left(1 - \frac{c\rho}{T^3}\right)\left[\frac{1}{\rho} + B_0(1 - b\rho)\right] - A_0\rho^2(1 - a\rho) \tag{25.1}$$

where
- R is the ideal gas constant (=8.314 J/mol K)
- the pressure P is expressed in Pa
- ρ is expressed in kg/m^3
- T is expressed in K
- the parameters a, b, and c are equal to -5.06×10^{-6} m^3/mol, -43.56×10^{-6} m^3/mol, and 5.04 m^3 K^3/mol, respectively
- the coefficients A_0 and B_0 are equal to 0.02 Pa m^3/mol^2 and 20.96×10^{-6} m^3/mol, respectively [30]

Figure 25.4 compares the actual density of hydrogen ρ with that predicted by the ideal gas law ρ = PM/RT for temperature and pressure ranging 48–398 K and 1–1000 bar (14.5–14,500 psi), respectively. It shows that H_2 deviates from ideal gas law for values of PM/RT larger than 10, that is, for low temperatures and/or high pressures.

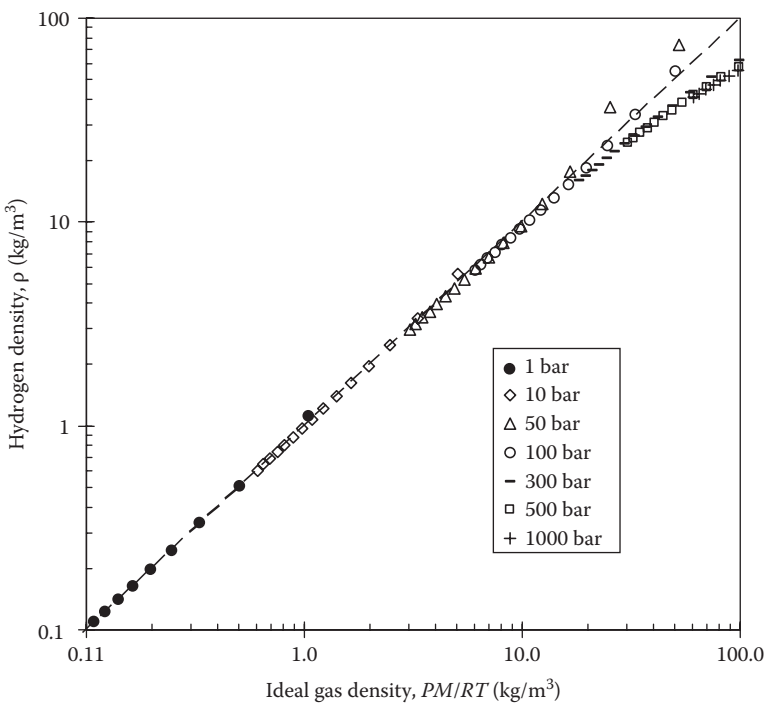

FIGURE 25.4
Actual hydrogen density versus ideal gas density (ρ = PM/RT) for pressure ranging from 1 to 1000 bar and temperatures between 48 and 398 K. (From Lemmon, E.W. et al., NIST reference fluid thermodynamic and transport properties database (REFPROP): Version 8.0, National Institute of Standards and Technology, Boulder, CO, http://www.nist.gov/srd/nist23.htm, 2007.)

Downloaded by [Laurent Pilon] at 06:37 11 August 2014

25.2.2.2 Compressibility Factor

Alternative to the previous equation of state, one can define the compressibility factor as

$$Z(T,P) = \frac{PM}{\rho RT} \tag{25.2}$$

Figure 25.5 shows the compressibility factor of hydrogen as a function of pressure P between 1 and 1000 bar for different values of temperature T between 48 and 398 K. Within this range, the compressibility factor $Z(T,P)$ of H_2 varies between 0.68 and 2.23. It is nearly equal to unity (ideal gas) for pressure less than 10 bar and temperatures larger than 48 K.

25.2.3 Burst Pressure

The volumetric energy density of hollow microspheres filled with hydrogen depends strongly on the differential pressure it can sustain. The maximum pressure of H_2 inside a hollow microsphere depends on the inner and outer radii denoted by r_i and r_o, respectively and on the biaxial tensile strength of the shell materials denoted by $\sigma_{s,max}$. For thin-walled microspheres (i.e., $r_o > 5(r_o - r_i)$), the burst pressure denoted by P_{max} is expressed as [31]

$$P_{max} = \frac{2\sigma_{s,max}(r_o - r_i)}{S_f r_0} \quad \text{for hollow microspheres} \tag{25.3}$$

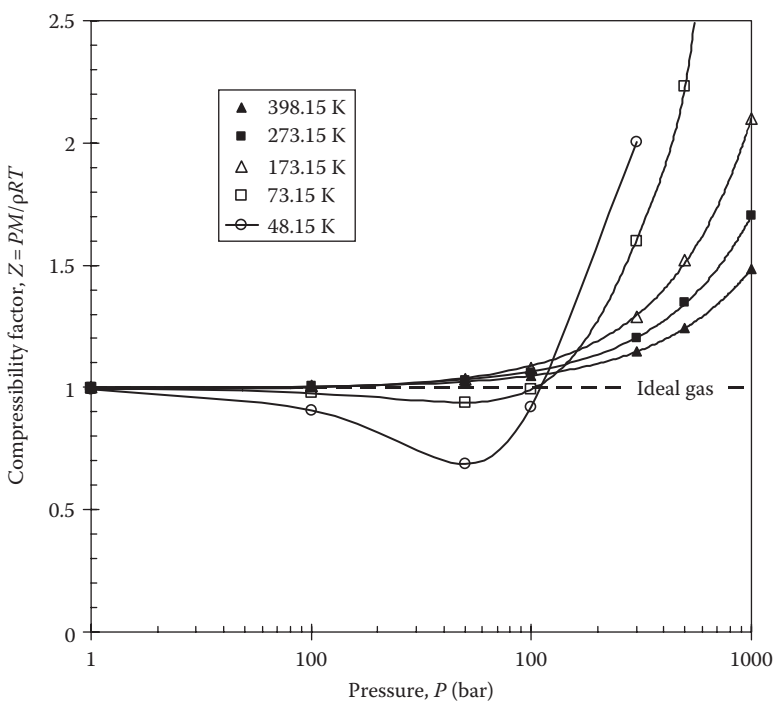

FIGURE 25.5
Compressibility factor of hydrogen as a function of pressure for temperature ranging from 48 to 398 K and pressure between 1 and 1000 bar. (From Lemmon, E.W. et al., NIST reference fluid thermodynamic and transport properties database (REFPROP): Version 8.0, National Institute of Standards and Technology, Boulder, CO, http://www.nist.gov/srd/nist23.htm, 2007.)

Downloaded by [Laurent Pilon] at 06:37 11 August 2014

A safety factor S_f, typically ranging from 1.5 to 10, must also be considered for the actual design and fabrication of the storage system [32]. It is often taken as 1.5 for H_2 storage applications since the breaking of one microsphere does not endanger the integrity of the entire hydrogen storage solution [32]. Equation 25.3 indicates that the internal pressure increases as the tensile strength $\sigma_{s,max}$ and the shell thickness $(r_o - r_i)$ increase and as the outer radius r_o decreases.

For cylindrical thin-walled containers, the burst pressure is expressed as [31]

$$P_{max} = \frac{\sigma_{s,max}(r_o - r_i)}{S_f r_0} \quad \text{for cylinders} \tag{25.4}$$

Here, $\sigma_{s,max}$ is the maximum strength in the radial direction also called hoop stress σ_h. For cylindrical geometry, a longitudinal stress σ_l exists but is only half the hoop (radial) stress, that is, $\sigma_l = \sigma_h/2$ [31]. It is evident from Equations 25.3 and 25.4 that hollow microspheres are, a priori, preferable to cylinders with the same inner and outer diameters as they can sustain burst pressures twice as large. However, synthesis of hollow microspheres is more challenging than microcylinders [4] (see Section 25.5).

Achieving large burst pressure first guided the search for the best shell materials that could stand large tensile stress. Teitel [9,10] suggested using glass for their outstanding mechanical properties under a wide range of temperatures. Indeed, the tensile strength of glasses is reported to be above 4 GPa and can reach up to 6.9 GPa for quartz (SiO_2) at room temperature compared with 460 MPa for steel [33,34]. Figure 25.6 shows the burst pressure predicted by Equation 25.3 for thin-walled microspheres as a function of radii ratio r_o/r_i

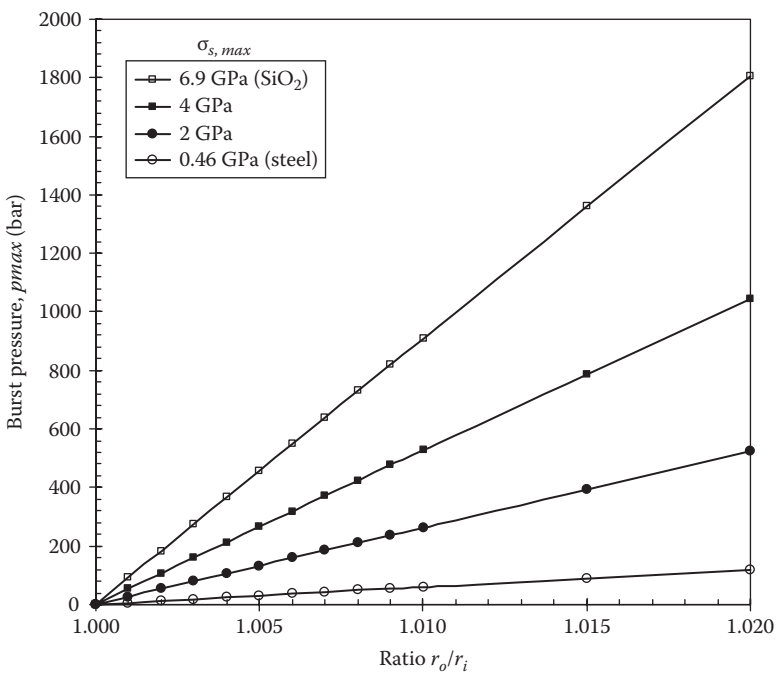

FIGURE 25.6
Burst pressure of thin-walled microspheres predicted by Equation 25.3 for different values of tensile strength $\sigma_{s,max}$ and $S_f = 1.5$. Burst pressure for cylinders with the same r_o/r_i ratio is half of that shown.

Downloaded by [Laurent Pilon] at 06:37 11 August 2014

for tensile strength σ_{max} varying from 460 MPa (steel) to 6.9 GPa (quartz) and safety factor equal to 1.5. The radii ratio r_o/r_i is kept smaller than 1.02, beyond which Equation 25.3 is no longer valid [31].

For either microspheres or microcylinders, the absence of defects in the sphere membrane (or shell) and the close-to-perfect sphericity or cylindricity are essential elements in order to achieve large burst pressure. Imperfection may exist and scratches can appear at the surface of the microcapsules during manufacturing and handling, which can result in decrease in the tensile strength [35]. To prevent scratches from occurring, the microcapsule surface can be acid etched or coated with a hard coating material as discussed in Sections 25.4 and 25.5.7.

25.2.4 Buckling Pressure

During hydrogen loading, the external pressure should be controlled to prevent the microspheres from collapsing when the difference between inner and outer pressures exceeds the buckling pressure. The classical expression for the static buckling pressure P_{cr} for isotropic thin-walled and shallow spherical shell under uniform pressure is given by [36,37]

$$P_{cr} = \frac{2E_s(r_o - r_i)^2}{r_o^2\sqrt{3(1-\nu_s^2)}} \tag{25.5}$$

where E_s and ν_s are the Young's modulus and Poisson's ratio of the shell material, respectively. The previous expression provides an upper limit for the pressure under which the hollow microspheres can be exposed [27]. In general, thin-walled microspheres can stand very large buckling loads [36]. In addition, numerous studies have also investigated dynamic buckling and how it is affected by shell defects, nonsphericity, nonuniformity in shell thickness, as well as coaxial loads [37–39]. However, experimental study for hollow microspheres were found to be more reliable to estimate the buckling pressure [37,39].

Rambach and Hendricks [27] experimentally investigated the buckling pressure of silicate glass microspheres 45 μm in average diameter and wall thickness of 0.9 μm. The buckling pressure predicted by Equation 25.5 was 1172 bar (17,000 psi) using E_s = 62.0 GPa and ν_s = 0.22. Experimentally, however, more than 20% of the microspheres collapsed for loading pressures larger than 500 bar at room temperature. Failure rate exceeded 80% for external pressure larger than 800 bar. No significant failure occurs for external pressure smaller than 414 bar (6000 psi) at the loading temperature up to 350°C thus setting practical limits of operations.

25.2.5 Hydrogen Permeation Processes

Gas permeability refers to the steady flow rate of gas across a specimen per unit of differential pressure and per unit thickness [40]. It is denoted by K and expressed in mol/Pa m s. The mass transfer rate of hydrogen entrapped in a single microsphere is expressed as [29]

$$\frac{dm_i}{dt} = \pm\frac{4\pi r_i^2 MK(T)}{(r_o - r_i)}(P_o - P_i) \tag{25.6}$$

Downloaded by [Laurent Pilon] at 06:37 11 August 2014

where P_i and P_o are the inner and outer pressures, respectively. The ± sign depends whether hydrogen is loaded (+) ($P_o > P_i$) or released (–) ($P_o < P_i$) from the microspheres. Here, changes in the surface area for diffusion were ignored, and the inner surface area $4\pi r_i^2$ was chosen since it is the smallest and therefore controls the hydrogen permeation [29]. The mass of H_2 contained inside the microspheres is given by [41,42]

$$m_i = \rho \frac{4\pi r_i^3}{3} = \frac{4\pi r_i^3}{3} \frac{P_i M}{Z(T, P_i)RT} \tag{25.7}$$

Similarly, for a single microcylinder, the mass transfer rate and the mass of H_2 entrapped are, respectively, expressed as

$$\frac{dm_i}{dt} = \pm \frac{2\pi r_i LMK(T)}{(r_o - r_i)}(P_o - P_i) \quad \text{and} \quad m_i = \frac{P_i M}{Z(T, P_i)RT} \pi r_i^2 L \tag{25.8}$$

where
L is the length of the cylinder
r_i and r_o are the inner and outer diameters, respectively

25.2.6 Geometric Considerations

Several geometric parameters should be optimized for hydrogen storage in microcapsules, namely, (1) the shape (spherical or cylindrical), (2) the inner and outer diameters r_i and r_o of the microspheres or microcylinders, (3) the shell thickness ($r_o - r_i$), and (4) the volume fraction or packing fraction ϵ of microcapsules in the storage tank, which depends on their size distribution. Each of these design parameters are discussed in the following sections.

25.2.6.1 Shape

Most studies have focused on hydrogen in hollow glass microspheres by virtue of the fact that microspheres have the highest burst pressure and smaller release time constant. In addition, glass was the material of choice for its high tensile strength and permeability. However, their synthesis can be more complex and costly than those of cylinders [4,20]. Yan et al. [20] manufactured hollow silica fibers with outer diameter ranging from 160 to 260 μm and wall thickness between 16 and 35 μm. The authors also discussed sealing and strengthening of the microcylinders (see Section 25.4)

25.2.6.2 Size

Commercially available hollow glass microspheres feature outer diameter between 5 and 500 μm and shell thickness between 0.5 and 20 μm [11]. Increasing the shell thickness increases the burst and buckling pressures and extends the hold time of the microspheres. However, it also reduces the volume available for hydrogen storage and the volumetric energy density while increasing the loading and unloading times. Thus, there exist an optimum values for outer and inner radii associated with operating temperature and pressure.

25.2.6.3 Packing Fraction

The maximum theoretical packing of monodisperse spheres is 74% corresponding to a body-centered (BCC) and face-centered (FCC) cubic face-centered arrangement as illustrated in Figure 25.7. However, this highly ordered arrangement is not achieved in practice

Downloaded by [Laurent Pilon] at 06:37 11 August 2014

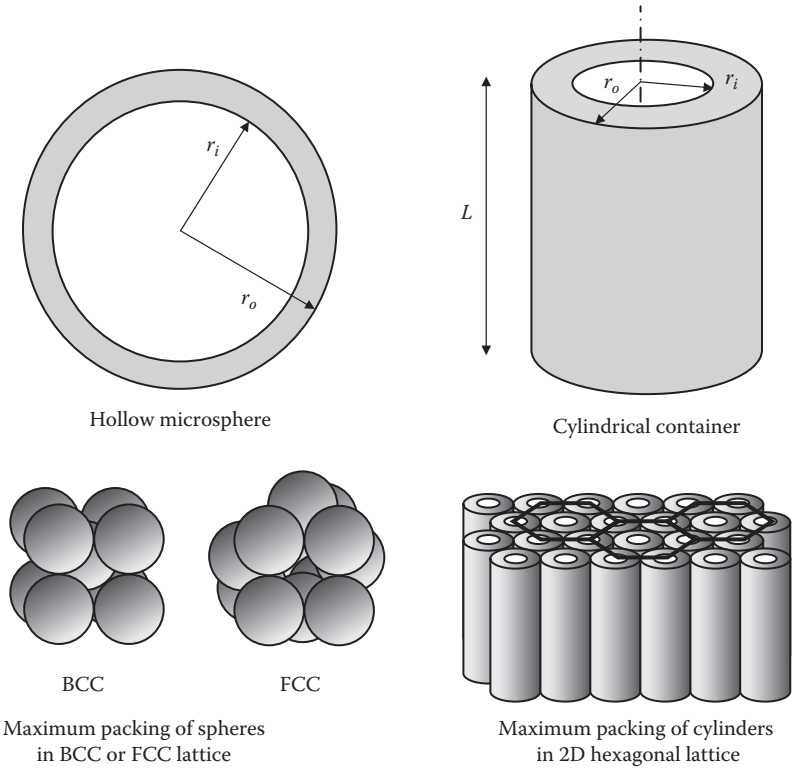

FIGURE 25.7
Schematic and dimensions of microspheres and microcylinders along with their spatial arrangement.

Downloaded by [Laurent Pilon] at 06:37 11 August 2014

and maximum random packing of 63.7% is more realistic [43]. Larger packing can be achieved if polydisperse spheres are used [43], but this can also complicate the handling, sorting, and recycling of the microspheres [11] since the microsphere density will vary with size, which is incompatible with the sink–float method [23,24].

Further increase in packing fraction can be obtained if the spheres are deformed or if polymeric or glass foams are used [21,44]. Pientka et al. [44] showed that extruded polystyrene foams can be used for hydrogen separation from CO_2 and N_2 as well as for hydrogen storage. Metallic foams can stand larger pressure than polymeric foams but have much larger density and may become brittle when exposed to H_2. Banyay et al. [21] concluded that metallic foams meet the volumetric energy density DOE target but not the gravimetric one and vice versa for polymeric foams. The authors suggested that composite foams might satisfy both targets. In the case of closed-cell foams for H_2 storage, Equation 25.6 is not valid and modeling mass transfer through foams has been discussed in the literature [45].

Finally, the maximum packing fraction of monodisperse and aligned cylinders ordered in 2D hexagonal lattice is 90.7% [4], while it is 0.82–0.83 if they are randomly packed [46].

25.2.7 Material Considerations

The shell material is selected for its tensile strength and permeability as a function of temperature along with the specific heat and optical properties depending on the heating process. These properties are reviewed in the following sections.

Downloaded by [Laurent Pilon] at 06:37 11 August 2014

25.2.7.1 Mechanical and Thermal Properties

Mechanical and thermal properties of glass depend on compositions, sample history, and temperature. Glass is brittle and much stronger under compression than tensile loads [47,48]. Table t-mechanics provides of range of realistic values for $\sigma_{s,max}$, E_s, ν_s, ρ_s, k_s, and $c_{p,s}$ [47]. Note that tensile strength is significantly affected by surface imperfections or flaws [47–49]. Strength of glass decreases as temperature increases [49]. It is also size dependent and strength of glass fibers increases sharply as the fiber diameter decreases, for example [48]. Attempts to correlate glass strength and composition were typically unsuccessful [48] and experimental data showed very large variations mainly due to the fact that surface flaws determine the glass strength and are difficult to observe directly [49]. The ultimate tensile strength $\sigma_{s,max}$ is expressed as [49,50]

$$\sigma_{s,max} = \sqrt{\frac{E_s \alpha}{a}} \tag{25.9}$$

where
E_s is the shell material Young's modulus
a is the interatomic distance
α is the surface energy

For commercial oxide glass, a is not significantly affected by the compositions [50] and is of the order of 2×10^{-10} m [49,50] while α varies from 3.5 J/m^2 for soda-lime glass to 5.2 J/m^2 for vitreous silica [49]. Thus, the ultimate tensile strength is 16 GPa for soda-lime silicate and 24 GPa for vitreous silica, for example. These values are much higher (up to 60% for silica [49]) than experimental measurements due to the unavoidable presence of surface flaws [49,50]. Thus, experimentally measured values of $\sigma_{s,max}$ should be used in estimating the burst pressure from Equation 25.3 (Table 25.2).

25.2.7.2 Hydrogen Permeability

The first mechanism for hydrogen dissolution in glass consists of physical dissolution when H_2 molecules occupy the interstices of the glass. The second mechanism involves

TABLE 25.2

Summary of Mechanical and Thermal Properties of Glasses Considered for Hydrogen Storage

Property	Vitreous Silica	Soda-Lime Glass	Borosilicate Pyrex
$\sigma_{s,max}$ (GPa)	24	16	14
E_s (GPa)	72.9–77.2	70–72	64
ν_s (-)	0.165–0.177	0.25	0.2
ρ_s (kg/m^3)	2200	2520	2230
$c_{p,s}$ (J/kg K)	712	754	750
$k_{c,s}$ (W/m K)	1.46–1.71	1.2–1.78	1.2–1.78

Source: Bansal, N.P. and Doremus, R.H., *Handbook of Glass Properties*, Academic Press, Inc., Orlando, FL, 1986.

chemical reactions between H_2 and the glass resulting in the formation of OH groups. For example, hydrogen causes the reduction of variable-valence ions such as Fe^{3+}, Ce^{4+}, and Sn^{4+} [51]. In particular, Fe^{3+} can be reduced almost completely to Fe^{2+} according to the following reaction [51]:

$$H_2 + 2(\equiv Si - O)^- + 2Fe^{3+} \rightleftharpoons 2(\equiv Si - OH) + 2Fe^{2+} \tag{25.10}$$

The reaction rate is much faster than the diffusion rate. Thus, the process is diffusion limited and can be accounted for through standard mass diffusion model with some effective diffusion coefficient, permeability, and solubility [52]. Several empirical relationships for temperature dependence of gas permeability $K(T)$ have been suggested and are of the following general form:

$$K(T) = K_0 T^n \exp\left(\frac{-Q_K}{T}\right) \tag{25.11}$$

where K_0, n, and Q_K are constants determined empirically. Souers et al. [53] identified K_0 and Q_K while n was set equal to 1 as suggested by Doremus [54] and Shelby [40]. Alternatively, other researchers [2,4,29,42,55–59] used the standard Arrhenius law for which $n = 0$. The values of K_0 and Q_K are sometimes expressed in terms of (1) the content of glass network formers such as SiO_2, B_2O_3, and P_2O_5 denoted by G and expressed in mol.% or (2) the content of modifier oxide such as CaO, Na_2O, MgO, SrO, and NaO denoted by M. Table 25.3 summarizes values of K_0 and Q_K as reported in literature for vitreous silica, silicate, soda-lime, and borosilicate glasses [29,53,55–58,60,61]. In general, hydrogen permeability increases with G and decreases with M as suggested by the expressions for Q_K reported in Table 25.3. In addition, the permeability has been reported in different units such as molecules/cm s atm and mol/cm s when measured with 1 atm pressure difference across the sample. Thus, conversion was sometimes necessary to compare the different studies according to

$$K\,(\text{in mol/Pa m s}) = \frac{100}{P_{atm} N_A} K\,(\text{in molecules/cm s atm}) = \frac{100}{P_{atm}} K\,(\text{in mol/cm s}) \tag{25.12}$$

where

N_A is the Avogadro number (=6.022 × 10^{23} molecules/mol)

P_{atm} is the atmospheric pressure (=1.013 × 10^5 Pa) or the pressure difference at which the measurements were performed

Note that H_2 permeability in glass can be considered to be independent of pressure up to 1000 bar [47]. Figure 25.8 shows the evolution of permeability as a function of temperature for the different glasses and references summarized in Table 25.3. It shows that H_2 permeability increases significantly with temperature and can vary widely with glass composition. It is also evident that permeability is systematically larger in vitreous silica or quartz than in glasses with other compositions.

Downloaded by [Laurent Pilon] at 06:37 11 August 2014

Downloaded by [Laurent Pilon] at 06:37 11 August 2014

TABLE 25.3

Empirical Constants for the Permeability of Various Glasses Used in Equation 25.11

Composition	n	$K_0 \times 10^{17}$ (mol/Pa m s)	Q_K(K)	References	Reported in
Soda-lime glass (72% ≤ G ≤ 100%)	0	8,100	17,330 − 127.8 G	[29]	mol/Pa m s
Silicate glasses	1	3.4 + 8 × 10^{-4} M^3	3,600 + 165 M	[53]	mol/Pa m s
Soda-lime glasses (M = 19%)	1	20	5,600	[53]	mol/Pa m s
Vitreous silica (see Ref. [40])	0	58.1	4,234	[55]	[a]
Vitreous silica (quartz)	0	8,688	4,469	[56]	molecules/cm s
Vitreous silica (quartz)	0	7,409	4,539	[57]	molecules/cm s
Pyrex (borosilicate) (D_2)	0	10.7	4,529	[58]	mol/cm s
Pyrex (borosilicate)	1	2.8	4,026	[60]	molecules/cm s atm
Pyrex (borosilicate) (D_2)	0	23.1	4,199	[61]	mol/cm s

[a] cc(STP)/s cm^2 area/mm thickness/cm Hg.

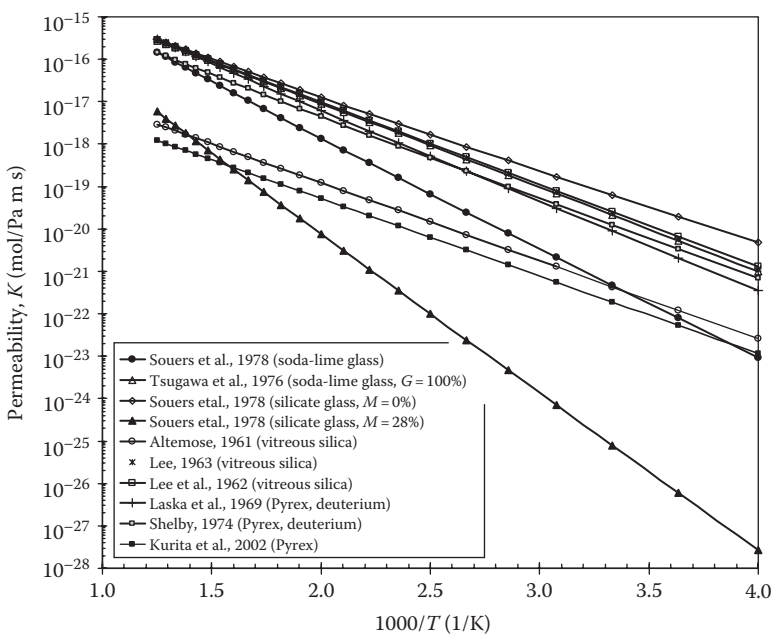

FIGURE 25.8
Hydrogen permeation through soda-lime, silicate, vitreous silica, and Pyrex as a function of 1000/T as reported in the literature and summarized in Table 25.3.

25.2.7.3 Hydrogen Diffusion Coefficient and Solubility in Glass

Diffusion coefficient $D(T)$ (in m^2/s) and solubility $S(T,P)$ (in mol/m^3 Pa) of hydrogen have also been reported in the literature for Pyrex [58,60], quartz [56–58], and silicate glass [59]. They are related to the permeability through [40]

$$K(T) = D(T)S(T) \tag{25.13}$$

They can be assumed to be independent of pressure below 1000 bar [47]. To be consistent with Equations 25.11 and 25.13, diffusion coefficient and solubility are expressed as

$$D(T) = D_0 T^n \exp\left(\frac{-Q_D}{T}\right) \quad \text{in}\, m^2/s \tag{25.14}$$

$$S(T,P) = \frac{K(T,P)}{D(T)} = S_0 \exp\left(\frac{Q_S}{T}\right) \quad \text{in}\, mol/Pa\, m^3 \tag{25.15}$$

where D_0, Q_D, S_0, and Q_S are empirical constants such that $K_0 = D_0 S_0$ and $Q_K = Q_D - Q_S$. Figure 25.9 shows the diffusion coefficient of vitreous silica and borosilicate Pyrex as a function of temperature as reported in the literature [40,57,61] and summarized in Table 25.4.

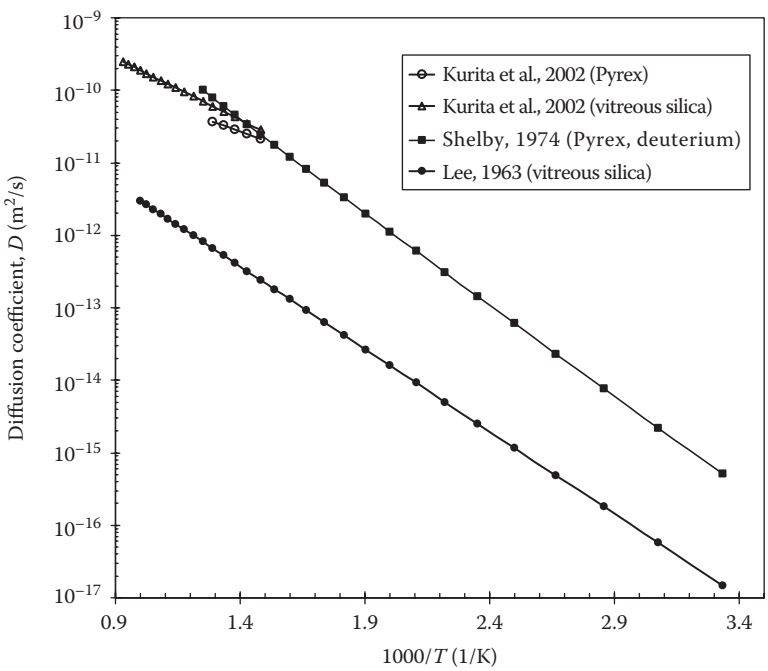

FIGURE 25.9
Hydrogen diffusion coefficient through vitreous silica and borosilicate Pyrex as a function of 1000/T as reported in the literature [40,57,61] and summarized in Table 25.3.

Downloaded by [Laurent Pilon] at 06:37 11 August 2014

TABLE 25.4

Empirical Constants for the Permeability of Various Glasses Used in Equation 25.14

Composition	n	$D_0 \times 10^{10}$ (m^2/s)	Q_D (K)	References	Gas
Vitreous silica	0	5.65	5237	[57]	H_2
Pyrex 7740	1	1.06	5385	[60]	D_2
Borosilicate Pyrex	0	14.0	2820	[61]	H_2
Vitreous silica	0	96.0	3928	[61]	H_2

Recently, Shelby et al. [62–65] presented experimental study of what they called *photo-induced hydrogen outgassing* from borosilicate glass doped with various metal oxides especially Fe_3O_4. The authors observed that [62–65] (1) hydrogen release from a slab of doped borosilicate glass placed in a vitreous silica tube was accelerated when exposed to an incandescent heating lamp compared with heating in a furnace at 400°C, (2) the onset of outgassing was observed immediately with lamp heating but was slower for furnace heating, (3) increasing the lamp intensity accelerated the H_2 release rate and the overall H_2 released from the sample, (4) borosilicate glass CGW 7070 demonstrated the best H_2 release response, and (5) increasing the Fe_3O_4 doping level increases the H_2 release rate. The authors suggested that "infrared radiation is contributing the activation energy necessary for hydrogen diffusion." To the best of our knowledge, this would constitute a new physical phenomenon [66]. It remains unclear, however, how the total irradiance and the spectral nature of radiation would be accounted for in an Arrhenius type of relation for the diffusion coefficient or permeability. Moreover, the reported experimental data do not isolate the proposed mechanism from the well-known thermally activated gas diffusion. In fact, Kitamura and Pilon [67] numerically showed that the experimental observations can be qualitatively explained based on conventional thermally activated gas diffusion and by carefully accounting for the participation of the silica tube to radiation transfer along with the spectral properties of the silica tube and the glass samples. In brief, the radiation emitted by the incandescent lamp has a peak emission between 1 and 2 μm and reaches directly the sample since the silica tube is nearly transparent up to 3.5 μm. On the contrary, for furnace heating at 400°C, the silica tube absorbs a large fraction of the incident radiation, which reduces the heating rate and the H_2 release rate. However, between 0.8 and 3.2 μm, undoped borosilicate does not absorb significantly. Coincidentally, Fe_3O_4 doping increases the absorption coefficient and also reacts with H_2 to form ferrous ions, which increase the absorption coefficient of the sample by two orders of magnitude. Thus, doped and reacted samples heat up much faster when exposed to the heating lamp resulting in the observed faster response time and larger H_2 release rate.

25.2.7.4 Optical Properties

In the case when heating of microcapsules is achieved by infrared lamp heating, the optical properties of the glass shell are essential to predict the heating rate and the temperature on which hydrogen permeability depends. Optical properties of fused quartz (vitreous silica) from ultraviolet to infrared at room temperature have been reviewed by

Downloaded by [Laurent Pilon] at 06:37 11 August 2014

Kitamura et al. [68]. Those of soda-lime silicate glass can be found in Ref. [69] while De Sousa Meneses et al. [70] reported the optical properties of borosilicate glass at room temperature over the spectral range beyond 4.0 μm.

As a first-order approximation, one can assume that glass optical properties do not change significantly with temperature (see Ref. [69], Fig. 2). However, they may change with ions doping and due to reaction with hydrogen. For example, in soda-lime silicate glass, Johnston and Chelko [51] established that reduction of Fe^{3+} by H_2 into Fe^{2+} results in significant increase in the absorptance of the glass sample in the spectral range from 0.4 to 2.5 μm. The changes were apparent with the unaided eye. Similarly, Shelby and Vitko [71] observed (1) an increase in absorptance beyond 0.8 μm and (2) a reduction in absorptance between 0.4 and 0.8 μm for soda-lime silicate. Rapp [65] confirmed Shelby and Vitko's results for Fe_3O_4-doped borosilicate glass showing an increase in the Fe^{2+}/Fe^{3+} ratio as the duration of exposure to hydrogen gas increases [64]. This was attributed to the fact that the absorption band around 380 nm corresponds to the ferric state (Fe^{3+}) while a peak around 1.1 μm corresponds to the ferrous state Fe^{2+}. In addition, the formation of OH groups results in a strong absorption band at wavelengths around 2.73–2.85, 3.5, and 4.5 μm [64,72,73]. The refractive and absorption indices of vitreous silica and borosilicate glass used in this study are presented in Figure 25.10.

Downloaded by [Laurent Pilon] at 06:37 11 August 2014

25.3 Performance Assessment

Several parameters are useful in assessing and comparing the performances of hydrogen storage solutions including hollow glass microspheres. Parameters of particular interest are (1) gravimetric and volumetric energy densities, (2) loading and unloading times, as well as (3) the energy required to store the hydrogen gas.

25.3.1 Gravimetric and Volumetric Energy Densities

The gravimetric energy density η_g of a bed of monodisperse hollow microspheres is expressed in MJ/kg and given by

$$\eta_g = \frac{N_T m_{H_2} \Delta H_L}{N_T (m_s + m_{H_2})} = \frac{\rho r_i^3 \Delta H_L}{\rho r_i^3 + \rho_s \left(r_o^3 - r_i^3 \right)} \tag{25.16}$$

where

N_T is the total number of microspheres in the container

m_s and m_{H_2} are the mass of the solid shell and of the entrapped H_2 in a single microsphere

The densities of H_2 and of the glass shell are denoted by ρ and ρ_s. The lower heating value (LHV) denoted by ΔH_L represents the amount of heat released from combusting a unit mass of H_2 at 25°C and returning the combusting products (H_2O) to 150°C. It is equal to 120 MJ/kg, which exceeds that of all conventional fuels including gasoline (42 MJ/kg), ethanol (27 MJ/kg), natural gas (47 MJ/kg), and coal (23 MJ/kg) [8]. Note that the mass of the container is not considered here since it can be a lightweight plastic whose mass is negligible compared with that of the microspheres.

Downloaded by [Laurent Pilon] at 06:37 11 August 2014

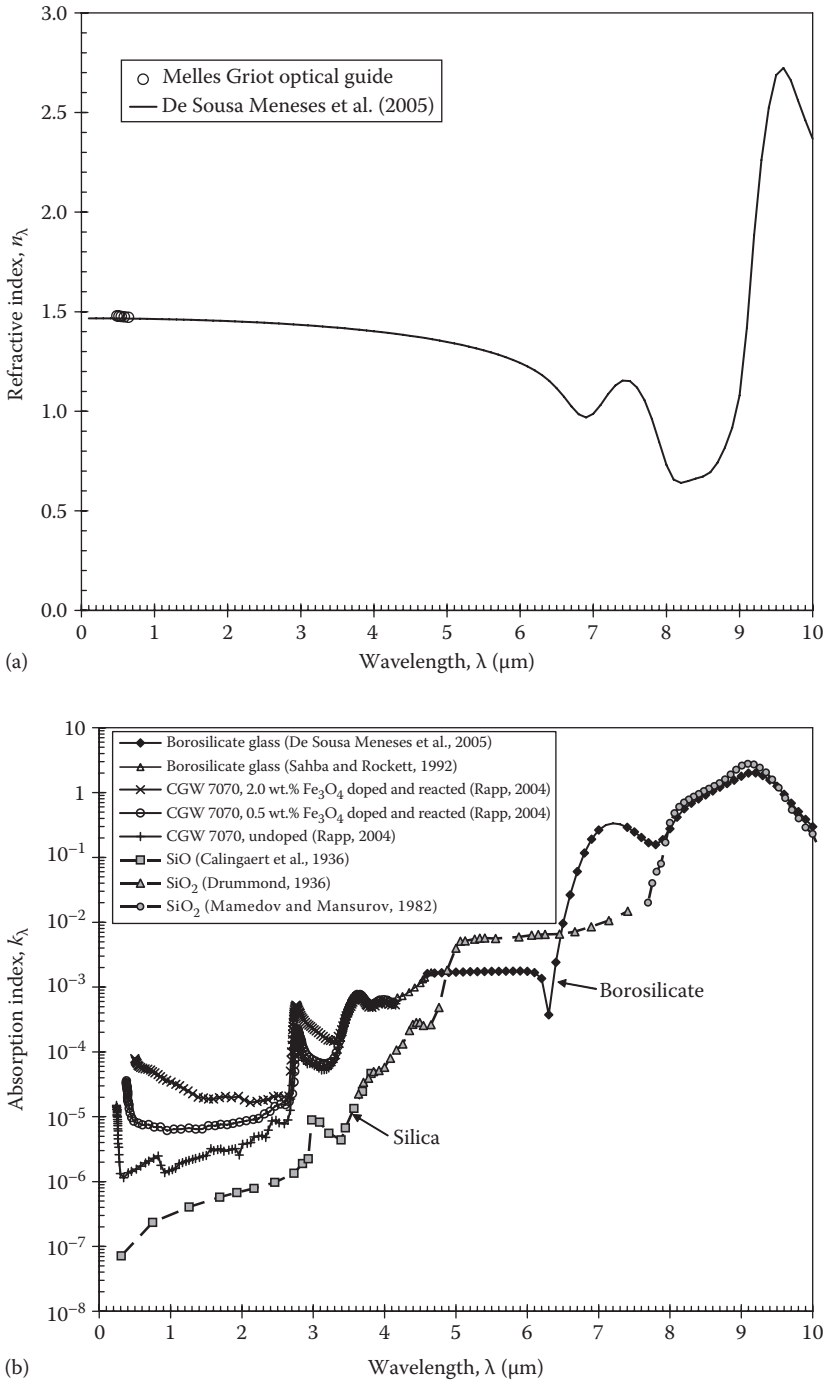

FIGURE 25.10
The (a) refractive and (b) absorption indices of undoped and Fe_3O_4 borosilicate glass obtained or retrieved from various sources. (From Rapp, D.B., Photo-induced hydrogen outgassing of glass, PhD thesis, Alfred University, Alfred, NY, 2004; De Sousa Meneses, D. et al., *J. Non-Crystal. Solids*, 351, 124, 2005; Sahba, N. and Rockett, T.J., *J. Am. Ceramic Soc.*, 75(1), 209, 1992.)

Similarly, the volumetric energy density η_v for monodisperse spheres is expressed in MJ/m^3 and given by

$$\eta_v = \frac{N_T m_{H_2} \Delta H_L}{N_T V_{total}} = \rho \epsilon \Delta H_L \left(\frac{r_i}{r_o} \right)^3 \tag{25.17}$$

where
V_{total} is the total volume of the storage solution
ϵ is the packing fraction of the hollow glass microspheres

Alternatively, the storage capacity and the hydrogen relative weight content have been used extensively to assess the performance of storage solutions [2,11]. The relative weight percent of hydrogen in the microsphere, expressed in kg of H_2 per kg of microspheres or wt.%, is defined as

$$\gamma_g = \frac{m_{H_2}}{m_s} = \frac{\rho r_i^3}{\rho_s (r_o^3 - r_i^3)} \tag{25.18}$$

Making use of the equality $(r_o^3 - r_i^3) = (r_o - r_i)(r_o^2 + r_i r_o + r_i^2) \approx 3 r_i^2 (r_o - r_i)$, γ_g simplifies to [2]

$$\gamma_g \approx \frac{\rho r_i}{3 \rho_s (r_o - r_i)} \tag{25.19}$$

Based on Equation 25.19, γ_g can be expressed in terms of burst pressure and tensile strength of the shell materials:

$$\gamma_g = \frac{2 \rho \sigma_{s,max}}{3 \rho_s S_f P_{max}} \tag{25.20}$$

On the other hand, the effective density of hydrogen stored in a bed of monodisperse hollow microspheres, expressed in kg of H_2/m^3 of bed, is given by [35]

$$\gamma_v = \frac{\eta_v}{\Delta H_L} = \rho \epsilon \left(\frac{r_i^3}{r_o^3} \right) \tag{25.21}$$

Note that because the shell thickness is relatively thin, $r_i^3 \approx r_o^3$ and γ_v depend essentially on the internal hydrogen pressure.

Figure 25.11 shows the gravimetric and volumetric energy densities of hydrogen stored at 300 K in randomly packed $(\epsilon = 0.63)$ monodisperse hollow glass microspheres 50 μm in diameter with shell thickness of 1 μm. The glass tensile strength $\sigma_{s,max}$ was taken as 1 GPa. It indicates that even for a conservative value of $\sigma_{s,max}$, hollow glass microspheres can achieve the 2015 DOE target for gravimetric energy density. Unfortunately, the volumetric energy density falls short of the 2015 DOE target by a wide margin unless the internal pressure greatly exceeds 1000 bar, which would require a large amount of energy for compressing H_2.

Downloaded by [Laurent Pilon] at 06:37 11 August 2014

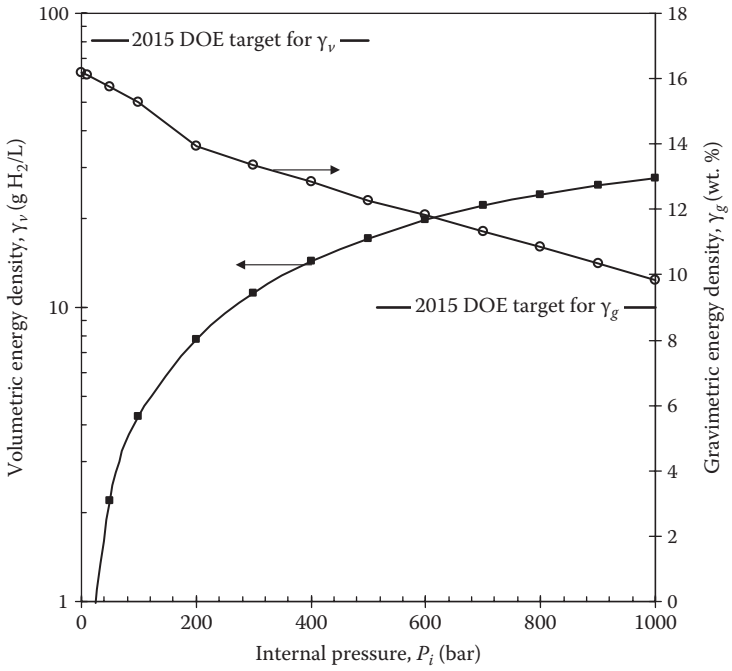

FIGURE 25.11
Gravimetric and volumetric energy densities of hydrogen stored in monodisperse hollow glass microspheres with r_o = 25 μm, $r_o - r_i$ = 1 μm, S_f = 1.5, $\sigma_{s,max}$ = 1 GPa, ε = 0.63, and ρ_s = 2230 kg/m³.

Finally, if the storage bed consists of monodisperse microcylinders with inner and outer diameters r_o and r_i, the gravimetric and volumetric energy densities are expressed as

$$\gamma_g = \frac{\rho r_i^2}{\rho_s(r_o^2 - r_i^2)} \quad \text{and} \quad \gamma_v = \rho\epsilon\left(\frac{r_i^2}{r_o^2}\right) \tag{25.22}$$

25.3.2 Loading and Unloading Times

Combining Equation 25.6 with equation of state (25.2) yields the following governing equation for the inner H_2 pressure:

$$\frac{d}{dt}\left(\frac{P_i}{Z(T,P_i)T}\right) = -\frac{3RK(T)}{r_o(r_o - r_i)}(P_o - P_i) \tag{25.23}$$

Then, assuming that the temperature T and the outer pressure P_o remain constant during the loading or unloading processes while the compressibility factor $Z(T,P_i)$ is approximately constant for pressure varying between $P_i(0)$ and $P_i(t)$ yields expression for the pressure inside the microcontainers:

$$P_i(t) = P_i(0) \pm [P_i(0) - P_o]exp\left(-\frac{t}{\tau}\right) \tag{25.24}$$

where the time constant τ is expressed as

$$\tau = \frac{r_i(r_0 - r_i)}{3Z(T,P_i)RTK(T)} \quad \text{for hollow spheres} \tag{25.25}$$

Downloaded by [Laurent Pilon] at 06:37 11 August 2014

The time needed for the pressure difference ($P_i - P_o$) to decrease by 63% and 95% from its initial value is equal to τ and 3τ, respectively. The presence of the compressibility factor Z in the denominator suggests that H_2 release is faster for large temperatures and pressures when Z is greater than 1 (see Figure 25.5). Treating hydrogen as an ideal gas at temperature T and pressure P_i gives $Z(T,P_i) = 1.0$ and $\tau = r_o(r_o - r_i)/3RTK(T)$ as often encountered in the literature [11,29,53]. Similarly, Equation 25.24 is valid for cylindrical containers with a time constant given by

$$\tau = \frac{r_i(r_o - r_i)}{2Z(T, P_i)RTK(T)} \quad \text{for cylinders} \tag{25.26}$$

Note that τ is independent of the cylinder length L [4]. In addition, assuming that the container wall is thin, the time constant for a sphere is 33% smaller than that for a cylinder with the same inner and outer diameters. In other words, loading and unloading times are shorter for spheres than for cylinders. The maximum shelf time of loaded microcapsules can be estimated from Equations 25.25 and 25.26 using $T = 300$ K. If the temperature of the microcontainer is not constant during the loading or unloading processes, the energy conservation equation must also be solved giving the temperature distribution within the container shell or within the packed bed. Heat transfer in packed beds has been studied extensively [74–85]. Models accounted for combined heat conduction through the wall of the hollow microspheres as well as for absorption, scattering, and emission of radiation models found in the literature can be adapted to predict the temperature inside a bed of hollow glass microspheres heated by a resistive heater or an incandescent lamp.

Figure 25.12 shows the evolution of the time constant τ as a function of temperature predicted by Equation 25.25 using permeation $K(T)$ reported by Lee et al. [56] for hollow vitreous silica microspheres 50 μm in diameter with shell thickness equal to 1 μm, that is, $r_o = 25$ μm and $r_o - r_i = 1$ μm. It also shows the time constant τ if the gas is assumed to be ideal, that is, $Z(T,P) = 1$. Note that for pressure less than 100 bar (1450 psi), the loading and unloading time is independent of pressure as observed experimentally with soda-lime glass [29]. However, when the initial hydrogen pressure is large ($Z(T,P) > 1$), the time constant depends on pressure and is shorter than that predict assuming ideal gas behavior.

Figure 25.13 shows the loading and unloading characteristic time τ as a function of the microsphere radius r_o at temperatures corresponding to (1) storage and handling temperature (25°C) and (2) the loading and unloading temperatures of 200°C and 400°C assuming that the shell is 1 μm thick and made of vitreous silica. It establishes that the loading and unloading time decreases significantly with decreasing microsphere radius and increasing temperature.

As previously mentioned, permeation is associated with the steady-state transport of hydrogen through the glass shell. Thus, it does not account for the time necessary for H_2 to diffuse through the shell of the microspheres before reaching a steady-state mass flux. This lag time denoted by τ_l corresponds to the time needed to establish the glass solubility in the microspheres wall. As a first-order approximation, τ_l can be expressed as [29]

$$\tau_l = \frac{(r_o - r_i)^2}{6D(T)} \tag{25.27}$$

where the lag time depends only on the shell thickness. It is typically much smaller than the unloading or loading time at low temperatures (i.e., $\tau_l \ll \tau$). For example, for hollow

Downloaded by [Laurent Pilon] at 06:37 11 August 2014

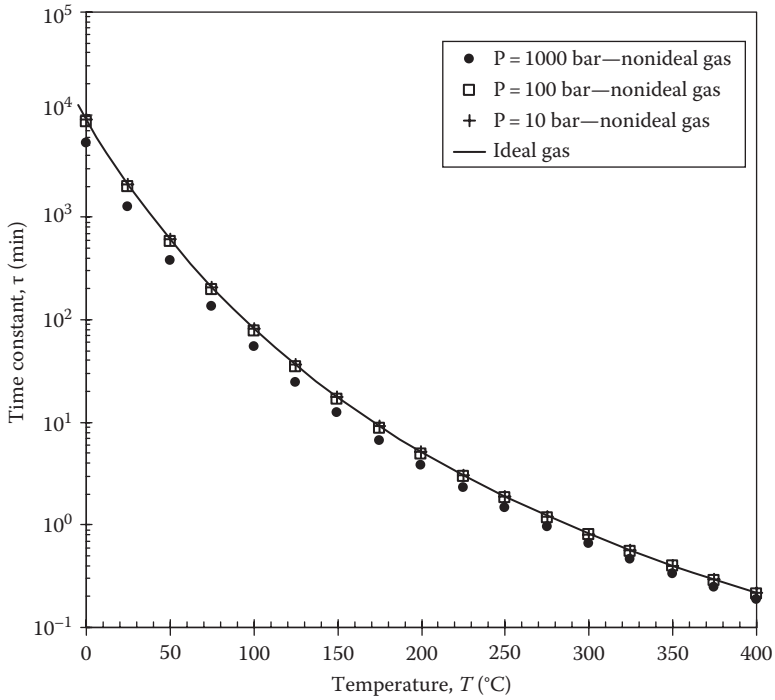

FIGURE 25.12
Loading and unloading time constant τ predicted by Equation 25.25 for vitreous silica glass microspheres with r_o = 25 μm, $(r_o - r_i)$ = 1 μm, $Z(T,P)$ = 1.0, $K_0 = 8.688 \times 10^{-14}$ mol/Pa m s, and Q_K = 4469 K. Time constant for microcylinders can be found by multiplying the results shown by 3/2. (From Lee, R.W. et al., *J. Chem. Phys.*, 36(4), 1062, 1962.)

vitreous silica microspheres with r_o = 25 μm and $(r_o - r_i)$ = 1 μm, the time constant τ is 0.9 days, 3.8 min, and 11 s compared with the corresponding time lag τ_l of 6.2 min, 0.3 s, and 7 ms at temperature of 25°C, 200°C, and 400°C, respectively. Nonetheless, this suggests that 95% of the hollow glass microspheres content is released in 33 s at 400°C and in 2.7 days at 25°C.

25.3.3 Filling and Discharging Energy Requirements

Another key element is assessing that the performance of hydrogen storage solution is (1) the energy required to compress the hydrogen gas to pressures in excess of 450 MPa during loading and (2) the thermal energy provided to heat up the microspheres and their content around 400°C to achieve high permeation rates.

Because of repulsion forces between H_2 molecules, hydrogen gas deviates significantly from an ideal gas under loading conditions and requires large compression work. Energy-efficient and cost-effective hydrogen compressors operating at high pressure are critical components of the envisioned hydrogen economy [86]. Hydrogen gas has also small molecules and low viscosity, which renders sealing of the compressors challenging. In addition, at high temperatures and pressures, hydrogen permeates through steel and causes embrittlement resulting in material failure, high maintenance costs, and safety concerns.

Downloaded by [Laurent Pilon] at 06:37 11 August 2014

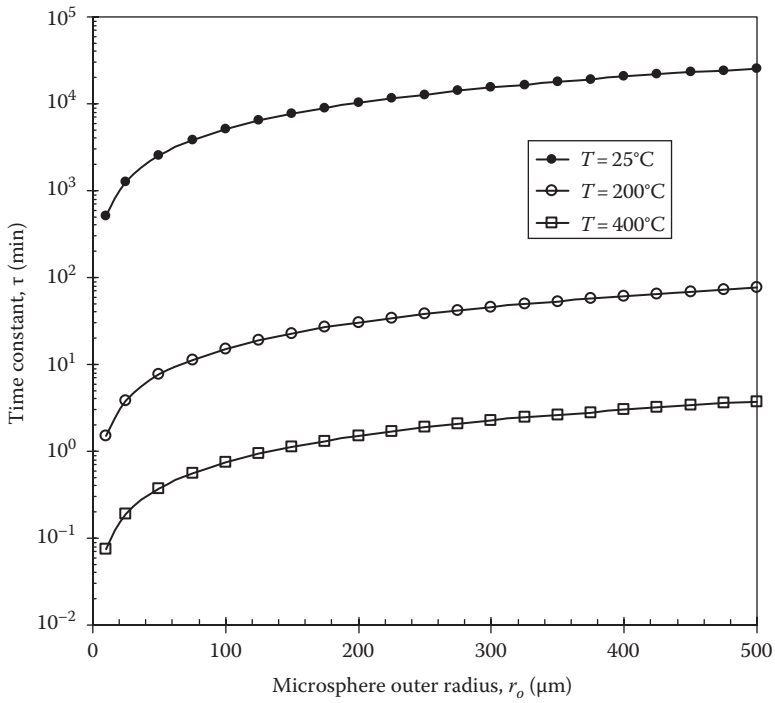

FIGURE 25.13
Loading and unloading time constant τ predicted by Equation 25.25 for vitreous silica glass microspheres as a function of r_o assuming $(r_o - r_i) = 1$ μm, $Z(T,P) = 1.0$, $K_0 = 8.688 \times 10^{-14}$ mol/Pa m s, and $Q_K = 4469$ K. (From Lee, R.W. et al., *J. Chem. Phys.*, 36(4), 1062, 1962.)

Downloaded by [Laurent Pilon] at 06:37 11 August 2014

Material embrittlement can be addressed by using more expensive material alloys such as chromium/molybdenum/vanadium alloys.

The total specific energy E_t required per loading and unloading cycle of 1 kg of microspheres with H_2 is the sum of (1) the specific work done for pressurizing the hydrogen during loading denoted by W_p and (2) the specific thermal energy for heating both the microspheres and the hydrogen to desired temperatures denoted by Q_u, that is,

$$E_t = W_p + 2Q_u \tag{25.28}$$

where the factor 2 accounts for thermal energy required for both loading and unloading.

The compression work required for pressurizing H_2 depends on the thermodynamic process, the number of stages, the compressor efficiency β, and the initial and final hydrogen pressures denoted by P_1 and P_2, respectively. For isothermal compression and assuming ideal gas behavior, the specific compression work W_p (in J/kg) is given by [86]

$$\beta W_p = -\int_{\rho_1}^{\rho_2} \frac{P(T,\rho)}{\rho^2} d\rho = ZRTln\left(\frac{\rho_1}{\rho_2}\right) \tag{25.29}$$

For isentropic compression, the specific compression work is expressed as [86]

$$\beta W_p = \frac{k}{(k-1)} \frac{P_1}{\rho_1} \left[\left(\frac{P_2}{P_1} \right)^{(k-1)/k} - 1 \right] \tag{25.30}$$

where
k is the specific heat ratio ($k = c_p/c_v$)
ρ_1 is the density at T_1 and P_2

Assuming hydrogen is compressed from standard temperature and pressure $\rho_1 = 0.09$ kg/m^3 and $k = 1.41$. Multistage compressors with cooling between stages operate between these two limiting cases albeit closer to isothermal [86]. Figure 25.14 shows the work W_p required for adiabatic and isothermal hydrogen compressions as a fraction of the hydrogen LHV as a function of final pressure P_2. For example, multistage compression from atmospheric pressure to 200 and 800 bar requires 11.9% and 19.1% of the LHV of hydrogen, respectively. It can reach 20% if one accounts for mechanical and electrical losses. These results are in good agreement with analysis by Ramback et al. [26,27,32]. The authors estimated the specific compression work for temperatures up to 400°C and pressure less than 620 bar to range between 10% and 20% of the LHV of H_2 assuming a three-stage compressor with 75% efficiency (Fig. 7 in Ref. [32]). However, Ramback [32] noted that it is less than the energy needed to liquify hydrogen, and therefore, hydrogen storage in hollow glass

Downloaded by [Laurent Pilon] at 06:37 11 August 2014

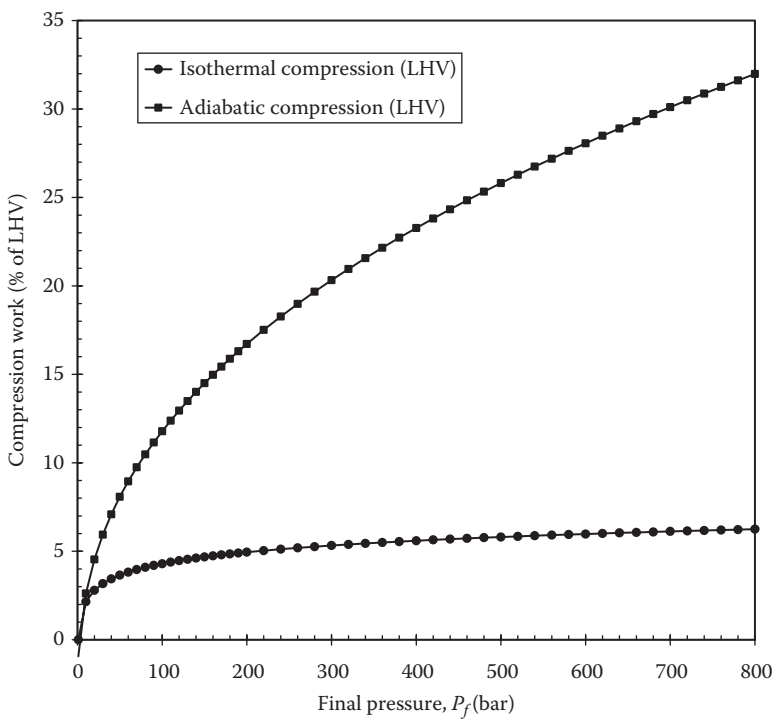

FIGURE 25.14
Energy required for adiabatic and isothermal compressions as a fraction of the hydrogen LHV.

TABLE 25.5

Expression of Design Parameters for Thin-Walled Monodisperse Hollow Microspheres and Microcylinders

Parameters	Symbol	Microspheres	Microcylinders
Burst pressure	P_{max}	$P_{max} = \frac{2\sigma_{s,max}(r_o - r_i)}{S_f r_0}$	$P_{max} = \frac{\sigma_{s,max}(r_o - r_i)}{S_f r_0}$
Buckling pressure	P_{cr}	$P_{cr} = \frac{2E_s(r_o - r_i)}{r_o\sqrt{3(1-\nu_s^2)}}$	$P_{cr} = \frac{E_s(r_o - r_i)}{r_o\sqrt{3(1-\nu_s^2)}}$
Maximum packing	ϵ	74%	90.7%
Random packing	ϵ	63%	82%–83%
Loading time constant	T	$\tau = \frac{r_i(r_o - r_i)}{3Z(T, P_i)RTK(T)}$	$\tau = \frac{r_i(r_o - r_i)}{2Z(T, P_i)RTK(T)}$
Gravimetric density	γ_g	$\gamma_g \approx \frac{\rho r_o^3}{\rho_s(r_o^3 - r_i^3)}$	$\gamma_g = \frac{\rho r_i^2}{\rho_s(r_o^2 - r_i^2)}$
Volumetric density	γ_v	$\gamma_v = \rho\epsilon r_i^3/r_o^3$	$\gamma_v = \rho\epsilon r_i^2/r_o^2$

microsphere can be economically competitive. On the contrary, Robinson and Iannicci [87] concluded that compressing H_2 at high pressures in excess of 1000 bar appears unpractical from an energy consideration point of view despite the fact that hollow glass microspheres could sustain such pressures [11]. Similar conclusions were reached by Bossel [86] and was identified as one of the reasons why the hydrogen economy *will never make sense*.

The specific thermal energy required to heat up the microspheres and the hydrogen from T_1 to T_2 can be expressed as

$$Q_u\,(\mathrm{J/kg}) = \int_{T_1}^{T_2} c_{eff}(T)\,\mathrm{d}T \tag{25.31}$$

where c_{eff} is the effective specific heat of the microcontainer bed defined as $c_{eff} = \epsilon[c_p r_i^3/r_o^3 - c_{s,p}(1 - r_i^3/r_o^3)]$. As a first-order approximation, one can assume c_{eff} to be constant so Q_u is proportional to the temperature difference ($T_1 - T_2$). Ramback [27] showed that it represents between 2% and 6% for monodisperse soda-lime silicate hollow microspheres 50 μm in diameter with a 0.9 μm thick shell for $\epsilon = 0.63$ and ($T_1 - T_2$) between 100°C and 400°C and pressures between 248 and 620 bar.

Table 25.5 summarizes expressions for design parameters and assessing performances of thin-walled monodisperse hollow microspheres and microcylinders.

25.4 Experiments

Only a few experimental studies focusing on H_2 storage in glass microcontainers have been performed over the last three decades and are summarized in Table 25.6. Teitel [9,10] performed crush tests and loading tests with different commercial hollow microspheres made of soda-lime silica glass with outer radius ranging from 14 to 55 μm and wall thickness from 0.4 to 2.2 μm. They showed that the survival rate varied from 30% to 90% depending

Downloaded by [Laurent Pilon] at 06:37 11 August 2014

TABLE 25.6

Summary of Experimental Studies on Hydrogen Storage in Microcapsules

References	Composition	Shape	r_o (μm)	$(r_o - r_i)$ (μm)	Loading P (bar)/T (°C)	Outgassing T(°C)	η_g (wt.%)	η_v (g/L)
[29]	Soda-lime	Microspheres	40–45	1	104	100–300	2	
[18]	Soda-lime	Microspheres	14–55	0.4–2.2	551/350	N/A	5.3	12
[20]	Fused quartz	Microcylinders	160–260	16–35	N/A	N/A	2	N/A
[35]	S60/1000 (3M)	Microspheres	5–15	200	350	4	14	
[27]		Microspheres	25.5	0.9	581/350			
[34]	Soda-lime	Microcylinders	100–500	2–10	100–250	200–250	15–17	10–15

2015 DOE targets are η_g = 9 wt.% and η_v = 81 g H_2/L.

Downloaded by [Laurent Pilon] at 06:37 11 August 2014

on the glass composition, the microsphere radii, and the loading gas. The authors suggested an aspect ratio $r_o/(r_o - r_i)$ of at least 30. Loading tests were performed at up to 551 bar (8000 psi) at 350°C. The author reported a gravimetric energy density of 4%–5% and a volumetric energy density of 20 g of H_2/L. Pressure would need to be significantly increased to reach the 2015 DOE target of 9 wt.% and 81 g of H_2/L. Microspheres breakage rate during the loading and unloading cycle was about 15%.

Tsugawa et al. [29] loaded soda-lime silicate microspheres 40–45 μm in outer diameter with a 1 ± 0.1 μm thick shell. The microspheres were placed in a highly impermeable beryllium container and heated at 763 K. Then, hydrogen was introduced and pressurized for 24 h until pressure reached 103 atm. The microspheres were quenched for 1 min in liquid nitrogen. The gravimetric energy density was reported as 2 wt.%. Finally, outgassing was performed at constant temperature ranging from 373 to 573 K. The authors also established experimentally that soda-lime glass microspheres pressurized with H_2 fill to only 82 vol.% instead of 100% with helium and 2% of H_2 remained inside the microspheres after outgassing.

Duret and Saudin [35] performed crush and burst tests on commercial hollow glass microspheres, provided from 3M and Saint Gobain, with outer diameter between 2 and 80 μm and a mean diameter between 12 and 30 μm. Hollow glass microsphere effective density was between 0.57 and 1.5 g/cm^3. The crush test was performed in water at 1000 bar for a few hours followed by a float test. Survival rate as low as 10% was recorded. Unbroken microspheres underwent a burst test at 200 bar and 400°C. 3M microspheres could sustain the crush test and achieved gravimetric and volumetric energy density of 4 wt.% and 14 g/L, respectively.

Recent studies have explored the use of hydrogen storage in microcylinders. First, Yan et al. [20] drew fused quartz hollow fibers (or microcylinders) 15 cm in length and with outer diameter ranging from 160 to 260 μm and wall thickness between 16 and 35 μm. They also subjected the fibers to chemical strengthening through hydrofluoric acid (HF) etching [88]. In addition, fiber coating with Shellac was performed. This reduced significantly the frequency of breakage and protected the fibers' surfaces from the effects of aging and handling. Different end sealing techniques were also tested including (1) heat treating the tip of fiber bundles in a furnace, (2) individual fiber sealing with an open flame, and (3) end plugging the fibers with colloidal silica. Flame sealing method provided the best sealing. The authors also performed hot static and dynamic fatigue tests and burst tests as well as hydrogen loading and unloading tests. They established that liquid-phase HF etching

significantly increases the tensile strength of the microcylinders and enables further control of the wall thickness. Finally, a gravimetric energy density of 2 wt.% was reported.

Kohli et al. [34] loaded soda-lime silicate glass hollow microspheres with aspect ratio $r_o/(r_o - r_i)$ ranging from 80 to 180 at outside pressure up to 250 bar and temperature of 200°C–250°C. They estimated the gravimetric energy density at 15–17 wt.% and volumetric energy density between 10 and 15 g/L (Fig. 4 in Ref. [34]).

Based on the previous discussion, it is evident that hollow glass microspheres are the microcapsules offering the best mechanical and gas permeation properties, which maximize gravimetric and volumetric energy densities and minimize loading and unloading times. The next section presents manufacturing processes for producing hollow glass microspheres.

Downloaded by [Laurent Pilon] at 06:37 11 August 2014

25.5 Synthesis of Hollow Glass Microspheres

Extensive efforts have been devoted to the fabrication of hollow glass microspheres for applications ranging from thermal insulation and fire retardant to lightweight composite materials for flotation and reinforced materials. They have also been used for viscosity modification, shrinkage reduction, and chemical resistance enhancement of plastics or paints, as well as for radiation shield [89]. Hollow microspheres made of materials other than glass have also been used to encapsulate drugs for controlled drug delivery or colorant or artificial flavor in food science. Thus, there exist numerous synthesis methods with different levels of control in the size distribution, shell thickness, material composition, mechanical properties, and throughput. The different synthesis processes have been reviewed extensively elsewhere [90–93] and this section is meant to give a relatively brief overview. In addition, numerous patents have been claimed for manufacturing, functionalizing, or strengthening hollow glass microspheres [94–110].

25.5.1 Hollow Microspheres in Fly Ash

Hollow glass microspheres have been observed in fly ash emanating from coal-fired power plants [90,111]. Indeed, coal particles injected in the furnace contain silica, sulfates, and other inorganic matter. As coal particles burn from the outside inward, carbon gets oxidized, and the remaining matter forms a molten glassy outer shell. The inner coal continues burning and releases gases such as carbon dioxide and sulfur oxides resulting from the oxidation of carbon and sulfates at high enough temperatures. These gases are entrapped in the molten glassy shell and blow it to produce a hollow microsphere, which solidifies as it exits the furnace. However, the hollow microspheres formed in this process (1) may not be perfectly spherical, (2) feature a wide size distribution (from a few to hundreds of microns), and (3) have nonuniform wall thickness [90]. Moreover, impurities and particles are often present in the shell along with tiny bubbles [90]. The nature of the process offers very little control except for the size of the initial coal particles [111].

25.5.2 Spray Pyrolysis Process

Several processes aimed to emulate hollow microspheres formation in coal burning but in a controlled manner have been developed over the last 50 years. The most widely used

processes can be reduced to two consecutive stages: (1) fabrication as semiproducts in the form of coarse or fine irregular particles or spheres and (2) blowing (or molding) of the semiproducts into hollow glass microspheres [92]. The main differences in the fabrication of hollow microspheres lie in the fabrication of the micropowder, which determines the dimensions and properties of the hollow glass microspheres. Formation of the semiproduct can include (1) glass frit, (2) liquid-droplet process, (3) solgel process, and (4) rotating and electric arc methods. The second stage consists of spray pyrolysis in flame or hot gas or a rotating electric arc plasma. Microspheres with porous walls have also been synthesized using spray pyrolysis [112,113].

25.5.2.1 Blowing Process

Glass frits, microspheres, or micropowders can be transformed in hollow microspheres using flame spray pyrolysis process [114]. It consists of spraying the semiproducts containing a blowing agent (e.g., sulfates) into an oxy-fuel flame at temperature between 1000°C and 1200°C. Upon rapid heating, the frit assumes spherical shape thanks to reduced viscosity and large surface tension. Beyond a certain temperature, the blowing agent undergoes thermal decomposition releasing gases (e.g., SO_2 and O_2), which results in the formation of a cavity that expands over time. Then, the resulting spherical hollow glass microspheres are rapidly cooled from the outside, which provides enough mechanical strength to retain their sphericity. The glass composition as well as the microsphere size and wall thickness can be controlled by changing the size, shape, and composition of the initial glass frit including the blowing agent [101,115,116]. Further control can be achieved through process parameters such as the residence time and the temperature history. Figure 25.15 shows the history of the semiproduct (e.g., glass frit or spherical particles) undergoing flame spray pyrolysis.

Other blowing processes have been proposed such as replacing flames by high-temperature gases. Similarly, Bica [117] formed hollow glass microspheres from glass frit introduced in a rotating electric arc plasma. The author reported that 85% of the glass frit was transformed into hollow microspheres with diameters between 2 and 24 μm and wall thickness between 0.4 and 1.6 μm.

25.5.2.2 Semiproduct Production

Glass frits are the simplest semiproducts used to produce hollow glass microspheres. They are obtained by mechanically crushing glass or by rapidly cooling hot glass, which shatters under thermal stress. Glass beads can also be produced from a stream of molten glass using (1) a horizontal rotating paddle wheel [118] to mechanically break

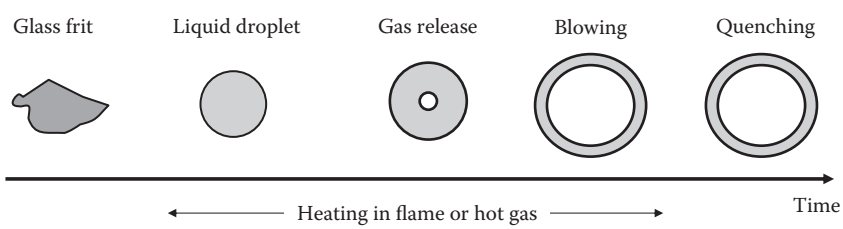

FIGURE 25.15
Schematic of a spray pyrolysis process to produce hollow glass microspheres.

Downloaded by [Laurent Pilon] at 06:37 11 August 2014

the vertically flowing stream or (2) under electric field in the longitudinal direction of the stream and a temporally variable magnetic field perpendicular to the stream [119]. However, the resulting glass frit has irregular shape and wide mass and size distributions. Consequently, the resulting hollow microspheres produced after the blowing process have also a widespread size distribution and shell thickness. Thus, a more advanced process has been conceived to produce semiproducts with controlled size and composition.

In dried-gel process, a gel having the desired glass composition is formed, dried, and ground into fine particles. Then, spray pyrolysis of the sieved gel powder (as opposed to glass frit) is performed. For example, Downs and Miller [120] claimed a solgel process resulting in a glass shell composed of at least 99% silica that does not suffer from inhomogeneities and phase separation associated with multiple component glass shells. A blowing agent such as urea may also be added to produce large hollow microspheres with thin wall [121]. Figure 25.16 shows micrographs of dried-gel particles and the resulting hollow glass microspheres after

However, dried-gel process tends to produce hollow microspheres with a wide range of diameter and wall thickness as illustrated in Figure 25.16. This drawback has been addressed by pressing the gel powder into mold to form cylindrical pellets of uniform and arbitrary size [122]. Moreover, Schmitt et al. [123] produced iron-doped sodium borosilicate

Downloaded by [Laurent Pilon] at 06:37 11 August 2014

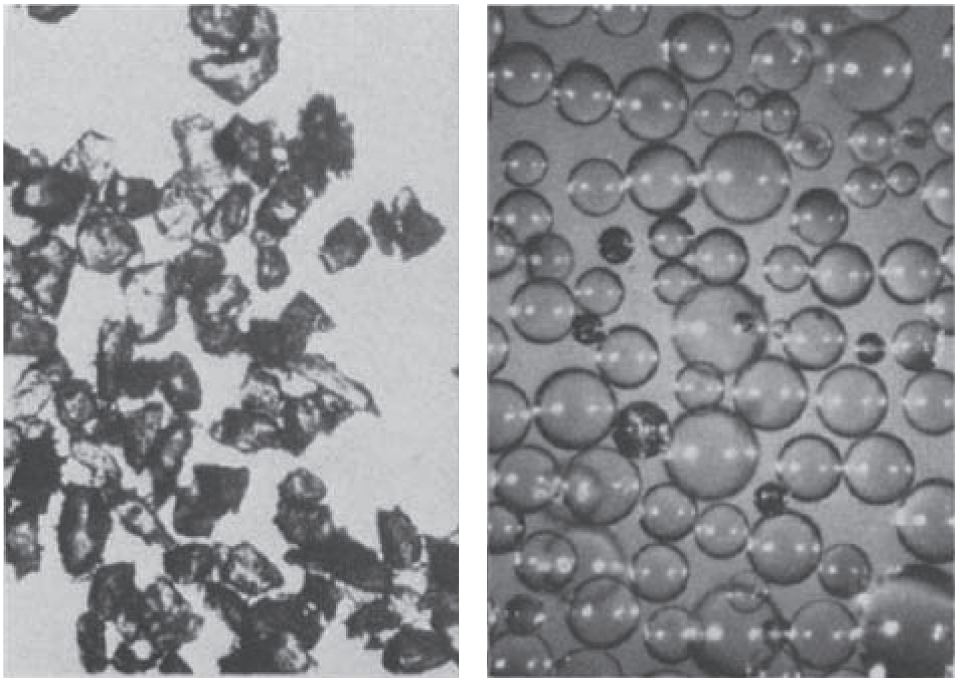

(a) (b)

FIGURE 25.16
Micrographs of (a) dried-gel particles and (b) resulting hollow glass microspheres after spray pyrolysis. (Reproduced from Hendricks, C.D., *J. Nuclear Mater.*, 85–86(1), 107–111, 1979; Rosencwaig, A. et al., Laser fusion hollow glass microspheres by the liquid-droplet method, Lawrence Livermore Laboratory Report UCRL-81421, June 5, 1978.)

granules doped by spray drying an aqueous suspension of crushed xerogel powder with iron chloride or iron sulfate and surfactants. They investigated the effects of heat treatment of the gel, spray drying parameters, and blowing agents.

25.5.3 Liquid-Droplet Method

Liquid-droplet process to produce glass beads to be blown into hollow microspheres was developed for producing laser fusion targets [121,124–126]. Figure 25.17 shows a schematic of the vertical-drop tower along with the different zones and thermal stages undergone by the liquid droplets. First, glass-forming components are dissolved and mixed in an aqueous solution. An in-line stream made of a large quantity of uniform-size droplets is generated by a Rayleigh–Taylor droplet generator [121,124,125] or a vibrating nozzle [121] at the top of a vertical-drop furnace. Air is drawn in the column in a controlled manner from the top to the bottom of the furnace. The generated droplets travel downward through a region of moderate temperature (region 1) to remove the water from the outer surface and to create an elastic gel membrane that encapsulates the rest of the droplet. Then, in region 2, water evaporates from the droplet and diffuses through the membrane resulting in dry solid gel particles. Upon further heating at higher temperatures (region 3), the gel

Downloaded by [Laurent Pilon] at 06:37 11 August 2014

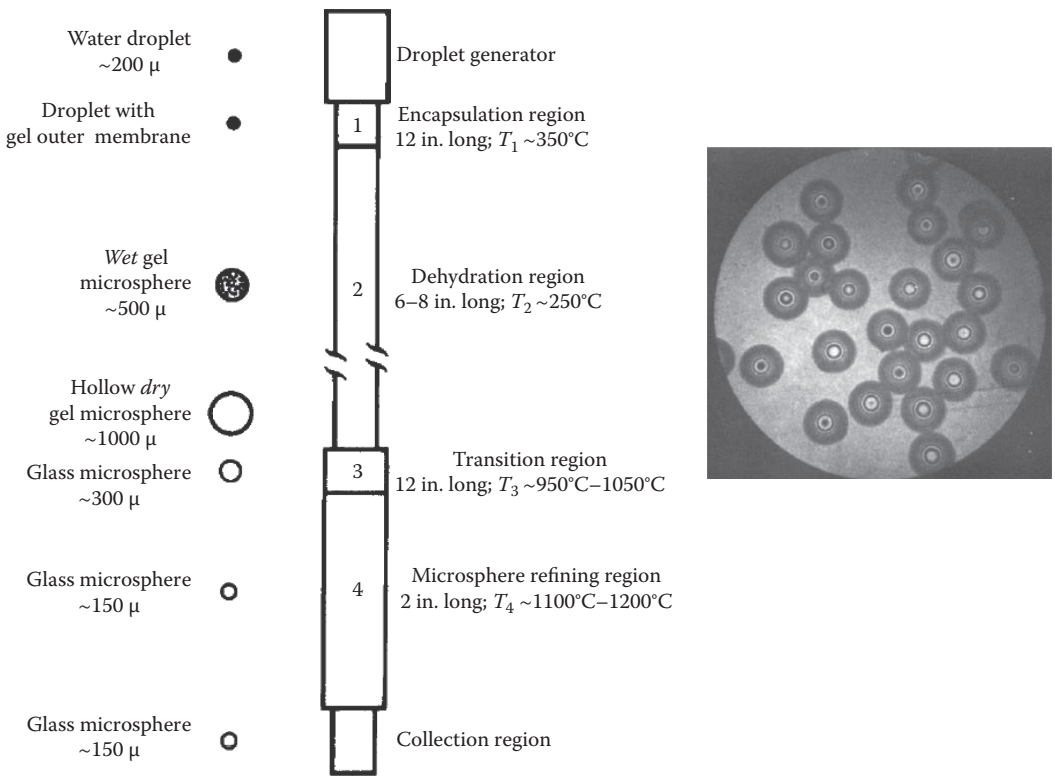

FIGURE 25.17
Schematic of a vertical-drop furnace used in liquid-droplet process and interference micrograph of the produced hollow glass microspheres. The column was 5 m high and made of quartz tube 7.5 cm in diameter. (Reproduced from Hendricks, C.D., *J. Nuclear Mater.*, 85–86(1), 107–111, 1979; Rosencwaig, A. et al., Laser fusion hollow glass microspheres by the liquid-droplet method, Lawrence Livermore Laboratory Report UCRL-81421, June 5, 1978.)

microspheres fuse to glass and collapse to form denser glass microspheres. In region 4, gases are released and diffuse through the shell whose wall becomes uniform thanks to lower viscosity caused by higher temperatures and to the action of surface tension forces. The hollow glass microspheres are then rapidly quenched and collected. This process produces nearly monodisperse microspheres with excellent sphericity, wall uniformity, and concentricity. It also offers control of the microspheres' diameter and shell thickness by controlling the liquid solution composition, the droplet formation process, the temperature profile in the column, and the liquid flow rate [91]. The microsphere size can be increased by increasing the drop tower height [121]. However, it requires that the glass-forming compounds be in solution. Unfortunately, some compositions form a gel so rapidly that droplets cannot be produced. In addition, the produced microspheres are small, spherical, monodisperse, and concentric as illustrated in Figure 25.17 [121]. However, the throughput is relatively small. Dried-gel process addresses the limitations in terms of composition, microsphere size, and throughput but has its own drawbacks as previously discussed [121,125].

Downloaded by [Laurent Pilon] at 06:37 11 August 2014

25.5.4 Hollow Glass Microspheres by Solgel Process

The synthesis of hollow glass microspheres by solgel process has been described by Ding and Day [127]. The starting aqueous solution is prepared with a precursor solution of metal alkoxide (e.g., tetraethyl orthosilicate [TEOS]) with ethanol and hydrochloric acid (HCl). Partial hydrolyzation (or polymerization) of the metal alkoxide, catalyzed by the acid, takes place over time. The solution is used to produce droplets with a droplet generator such as a vibrating nozzle [127]. The falling droplets are rapidly transformed into solid gel microspheres upon drying at temperatures less than 250°C. Finally, water, ethanol, and HCl are removed from the gel microspheres by thermal treatments at 500°C to 700°C to form hollow glass microspheres. Ding and Day [127] produced microspheres 60–81 μm in diameter. The advantages of this process include uniform sphere size, high chemical purity, low processing temperatures, and controllable microstructures along with the possibility of achieving compositions that cannot be made by conventional melting. Finally, hollow glass microspheres can also be synthesized using colloidal templating of sacrificial polystyrene latex microspheres removed by calcination [128] as well as miniemulsions [129].

25.5.5 Hollow Silica Aerogel Spheres

Hollow silica aerogel spheres have been synthesized by combining a droplet-generation method with solgel processing [130,131]. The process starts with preparation of TEOS, ethanol, and HNO_3 aqueous solution at pH 2. The solution is flown through the outer nozzle of a dual-nozzle hollow droplet generator. The hollow droplets are briefly injected in a gelation chamber where, upon contact with the gelation agent, they transform into rigid alcogel spheres. Two methods were proposed, namely, [130] (1) the levitation method where the droplets fall in an upward stream of NH_3–N_2 gas mixture acting as a gelation agent and (2) the NH_4OH vapor column techniques where the droplets fall through the saturated vapor above liquid NH_4OH. Both approaches are illustrated in Figure 25.18.

They are then collected and aged for 24 h in ethyl alcohol before being dried with supercritical CO_2. The process results in hollow silica aerogel spheres with a hollow core surrounded by a shell of silica aerogel and a thin outer membrane as shown in Figure 25.18. Spheres thus formed were several hundreds of microns in diameters and as large as 2 mm.

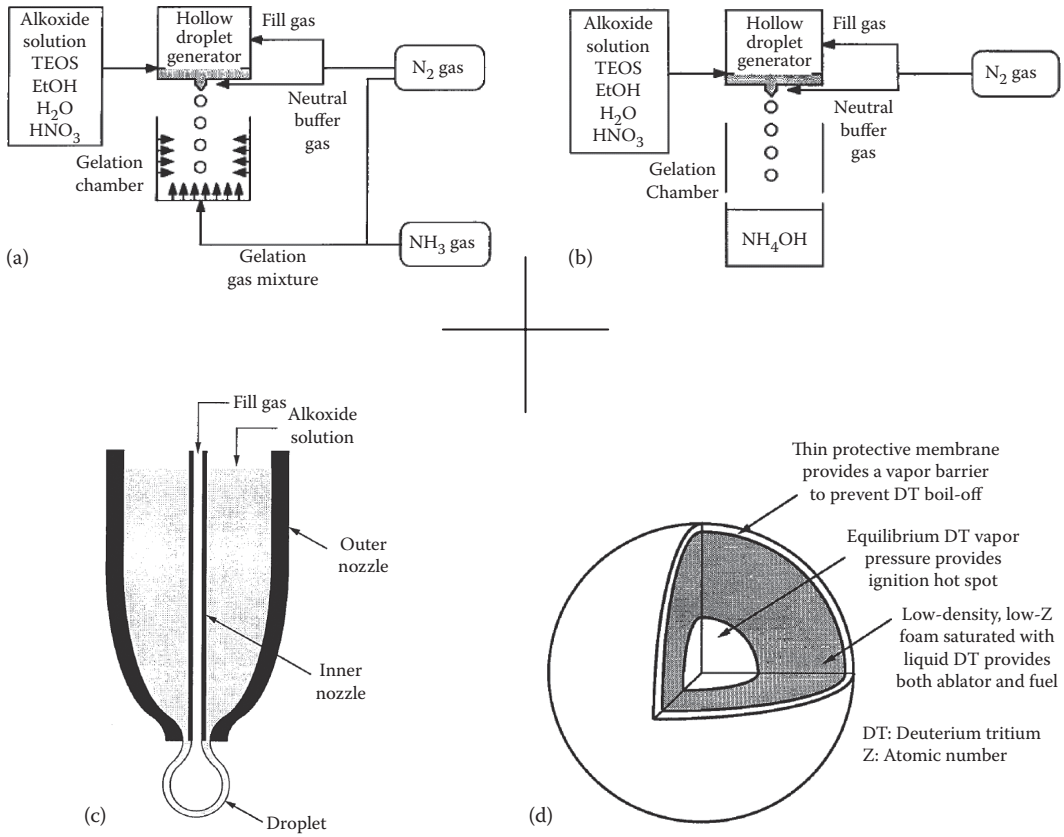

FIGURE 25.18
Illustration of hollow silica aerogel spheres synthesis method by (a) levitation in NH_3–N_2 gas mixture or (b) free fall in NH_4OH vapor column along with (c) dual-nozzle hollow droplet generator and resulting (d) hollow silica aerogel spheres. (Reproduced from Kim, K.K., *J. Am. Ceramic Soc.*, 74(8), 1987, 1991.)

Downloaded by [Laurent Pilon] at 06:37 11 August 2014

Porosity of the aerogel ranged from 90% to 97% with pore diameters between 9 and 60 nm. The porosity and pore size could be controlled by varying (1) the solution composition (and its viscosity), (2) the gelation time, and (3) the gelation method. Optimization of the process parameters were later investigated [131]. The overall diameter can be controlled through the design of the dual nozzle and the solution viscosity.

25.5.6 Porous Wall Glass Hollow Microspheres

More recently, porous wall glass microspheres made of silica glass containing boron oxide, alkaline earths, and alkali have been synthesized with diameters from 2 to 100 μm and shell thickness from 10 to 300 nm [112]. The first step of the process consists of flame spray pyrolysis to form conventional hollow glass microspheres. The shell is made porous through heat treatment and acid leached [112,113]. The heat treatment induces phase separation between a continuous silica-rich phase interconnected with an alkali- and borate-rich phase. Acid leaching with 3 M HCl at 80°C–85°C dissolves away the alkali–borate phase, thus making the wall porous with pore size between 1 and 100 nm. Figure 25.19 shows a schematic of the porous wall glass hollow microspheres along with an SEM

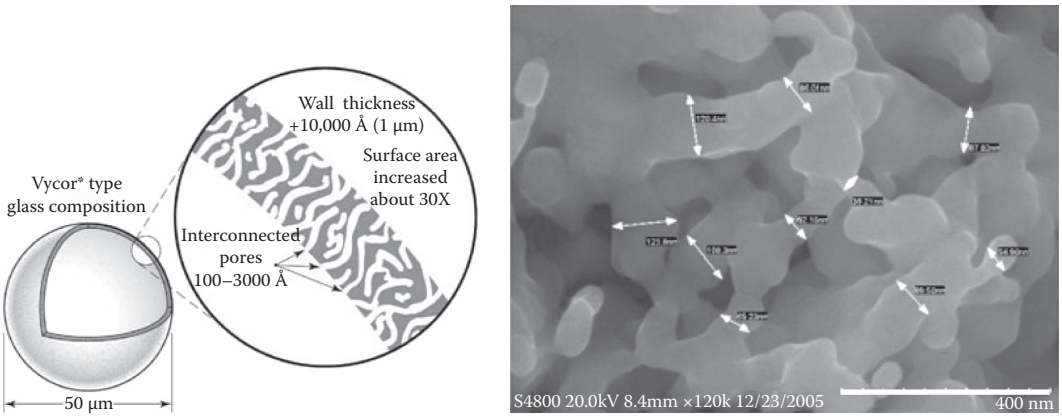

FIGURE 25.19
Schematic and SEM image of porous wall glass hollow microspheres. (Reproduced from Heung, L.K. et al., Hollow porous-wall glass microspheres for hydrogen storage, Patent Application No. US 2006/0059953 (October 21, 2005) and International Application No. PCT/US2006/040525 (October 17, 2006); Wicks, G.G. et al., *ACerS Bull*., 23–28, June 2008.)

picture of the porous wall. The porosity of the wall can be controlled by selecting different glass compositions and silica/alkali/borate ratios. The hollow microspheres can then be sorted by flotation techniques. Their density ranged from 0.1 to 0.7 g/cm^3. The authors were also able to fill the microspheres with palladium through the porous wall [113]. Thus, the microspheres could potentially be filled with various hydrogen adsorbent materials [113]. The porous wall would enable faster loading and release of the hydrogen.

Finally, alternative processes have been developed to synthesize hollow glass microspheres with porous wall combining (1) colloidal templating of polystyrene latex microspheres, to form a large microcavity with (2) solgel method to form the mesoporous wall after calcination of both the micelles and the microsphere [132–135]. Similarly, a combination of emulsions (e.g., oil/water) and the solgel method has been demonstrated by the self-assembly of silica and surfactants at the oil/water droplet interface [136,137]. In addition to pursuing these synthesis efforts, mechanical and thermal testing of these novel microspheres are needed including cycling under realistic pressures and temperatures expected during hydrogen loading and unloading.

25.5.7 Surface Treatment and Additional Functionality

As discussed in Section 25.2.7.1, tensile strength of the glass shell strongly depends on imperfection or flaws at the shell surface. Such flaws must be removed to strengthen and to improve the durability of the glass shell. Surface treatment by heat polishing [138] and chemical hardening [88] can be used to smoothen the microspheres' surface and strengthen their shell. Hendrick et al. [121] used a mixture of HNO_3 and NH_4F at 90°C followed by washes with water, acetone, and alcohol. Figure 25.20 compares SEM images of the surface of hollow glass microsphere commercially available with those synthesized and acid etched by Hendricks et al. [121,125].

The authors established that this etching process results in a 100–200 Å surface finish and no sign of surface deterioration after exposure to humid air compared with a few days when using conventional HCl or HF wash. Acid etching also provides further control of the shell thickness. In addition, processes have been developed for coating the hollow glass

Downloaded by [Laurent Pilon] at 06:37 11 August 2014

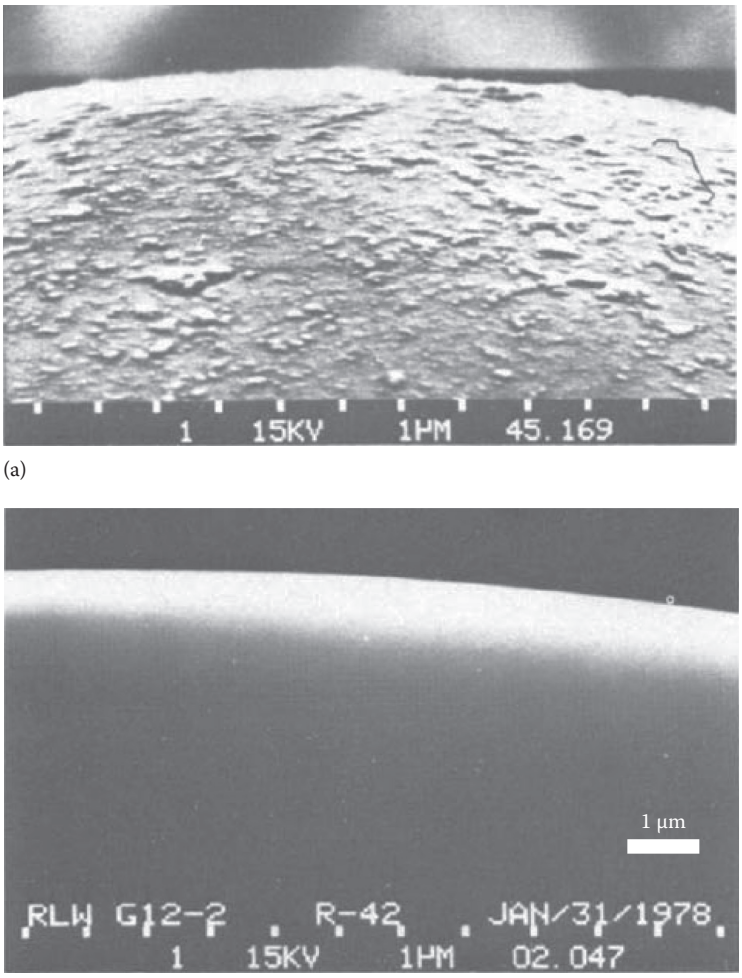

FIGURE 25.20
SEM images of the surface of hollow glass microsphere (a) commercially available and (b) synthesized by liquid droplet method and chemically etched. (From Hendricks, C.D., *J. Nuclear Mater.*, 85–86(1), 107–111, 1979.)

microspheres with a thin layer of materials to strengthen the thin glass shell [20,34,125,139]. For example, hollow glass microspheres have been coated with nickel [140], TiO_2, AlN [141], or with a gel [142] to name a few. Processes have also been developed to form a multilayer shell [143,144]. However, this protective coating should be thin and nonreactive with H_2 to limit potential barrier to hydrogen permeation. Acid etching and coatings of the shell of the hollow glass microspheres could be repeated between consecutive uses albeit at an additional cost.

25.5.8 Other Materials and Shapes

Hollow microspheres have also been made of polymers. They can be produced by emulsion processes as well as by coating solid template particles (e.g., polystyrene or silica) in liquid suspensions or in fluidized beds [91]. The solid particles act as sacrificial cores and

Downloaded by [Laurent Pilon] at 06:37 11 August 2014

are removed by thermolysis [91] or chemical etching. Hollow microspheres have also been synthesized with various polymeric materials and various size distributions [145–148].

As previously discussed, synthesis of cylindrical glass capillaries or hollow glass fibers is much more straightforward as they can be produced by simply drawing hollow fibers [149–151]. These products are inexpensive and commercially available as capillary tubes. For hydrogen storage, both cylinder ends must be sealed as described in details in Ref. [20].

25.6 Conclusions and Perspectives

This chapter has reviewed the principles, advantages, and challenges of hydrogen storage in hollow glass microspheres. Glass, and in particular vitreous silica, appears to be the material of choice for its superior tensile strength and good hydrogen permeability. In addition, hollow microspheres can sustain larger pressures and feature larger hydrogen permeation rate than cylinders with the same inner and outer radii and internal pressure. Significant progress has been made in synthesizing monodisperse hollow glass microspheres with controlled diameter and shell thickness. Strategies have been developed to further strengthen the shell through acid etching, heat polishing, or coating with hard material. Hollow glass microspheres feature excellent gravimetric energy density and can be safely handled at room temperature and atmospheric pressure and poured in any container solution. They are relatively inexpensive to make and the associated technology can be scaled up and present little risks. However, their volumetric energy density falls short of the 2015 DOE target. Moreover, the energy cost for compressing hydrogen at high pressure during loading is very high. Detailed cost analysis for this technology could not be found in the open literature. However, it has been stated that "the use of commercial grade hollow-glass microspheres for high pressure hydrogen storage has been shown to be cost ineffective" [7]. This conclusion was reached based on experimental tests performed by Teitel [18] and due to (1) material and synthesis cost, (2) the low volumetric energy density achieved, (3) high microsphere breakage rate, (4) the low fraction of recoverable hydrogen, and (5) the fill and release energy requirements. On the other hand, Akunets et al. [2] suggested that hydrogen storage in hollow glass microspheres could be used in applications when storage lifetime, safety, and weight are major concerns and where cost is not the determining factor. Similarly, Robinson and Handrock [7] suggested the use of hollow glass microspheres for fleet applications where volume and refueling concerns are not critical.

Based on the previous discussion and in order to make this technology competitive with other hydrogen storage technologies, the following technical recommendations are made [11,28]:

1. Develop energy-efficient, reliable, cost-effective, and clean 1000 bar hydrogen compressors [28]. Technologies to reduce energy requirement for H_2 compression would have no moving parts and be oil- and lubricant-free thus reducing the risk for contamination of hydrogen. They include metal hydride hydrogen compressors [152,153], for example. This effort would also benefit other high-pressure hydrogen storage technologies.
2. Develop inexpensive and high-throughput processes to produce high-quality monodisperse microspheres with large tensile strength and uniform shell thickness

Downloaded by [Laurent Pilon] at 06:37 11 August 2014

able to withstand high internal pressures. The shell material should also feature adequate permeability to achieve long dormancy time as well as short unloading times for on-demand delivery.

3. Optimize existing or develop new coating and etching techniques to strengthen the shell and reduce breakage rate during loading and handling. This would increase reliability and the number of loading and unloading cycles hollow glass microspheres can withstand.
4. Develop materials and strategies to unload H_2 at temperature below 100°C. Then, heating could be achieved by using waste heat generated by the fuel cell or a simple heater powered by a battery during fuel cell start-up.
5. Develop novel approaches to control H_2 permeability through nonthermal methods such as magnetic, electric, or electromagnetic [28].
6. Assess the financial and energy costs associated with reprocessing the spent microspheres.

Downloaded by [Laurent Pilon] at 06:37 11 August 2014

Nomenclature

a, b, c	Parameters in Bettie–Bridgeman equation
A_0, B_0	Parameters in Bettie–Bridgeman equation (=0.02 Pa m^3/mol^2)
c_p	Specific heat at constant pressure (J/kg K)
c_v	Specific heat at constant volume (J/kg K)
D	Diffusion coefficient (m^2/s)
D_0	Maximum diffusion coefficient (m^2/s)
E	Young's modulus of the shell material (Pa)
E_t	Specific total energy required for loading and unloading (J/kg)
ΔH_L	Hydrogen LHV (J/kg)
k	Ratio of specific heat, $\gamma = c_p/c_v$
k_c	Thermal conductivity (W/m K)
K	Permeability (mol/Pa m s)
K_0	Maximum permeability (mol/Pa m s)
L	Cylinder length (m)
M	Molar mass (g/mol) (=2.0158 g/mol)
P_{cr}	Buckling pressure (Pa or bar)
P_i	Inner shell pressure (Pa or bar)
P_{max}	Burst pressure (Pa or bar)
P_o	Outer shell pressure (Pa or bar)
Q_D	Specific thermal energy required for diffusivity (K)
Q_K	Specific thermal energy required for permeation (K)
Q_S	Specific thermal energy required for solubility (K)
Q_u	Thermal energy required for H_2 unloading (J/kg)
R	Universal gas constant (R = 8.314 J/mol K)
r_i	Inner shell diameter (m)
r_o	Outer shell diameter (m)
S	Solubility of hydrogen in shell material (mol/m^3 Pa)
t	Time (s)

T	Temperature (K)
W	Specific compression work (J/kg)
Z	Compressibility factor

Greek Symbols

α	Surface energy (J/m^2)
β	Compressor efficiency
γ_g	Gravimetric energy density (in wt.%)
γ_g	Volumetric energy density (in kg/L)
η_g	Gravimetric energy density (in MJ/kg)
η_v	Volumetric energy density (in MJ/L)
ν	Poisson's ratio of the shell material
ρ	Density of hydrogen gas (kg/m^3)
ρ_{eff}	Effective density of microcapsules (kg/m^3)
ρ_f	Density of the fluid in sink–float method (kg/m^3)
ρ_s	Density of the shell materials (kg/m^3)
σ_{max}	Tensile strength (Pa)
σ_h	Hoop stress (Pa)
σ_l	Longitudinal stress (Pa)
τ	Permeation time constant (s)
T_ℓ	Lag time constant (s)

Subscripts

i	Refers to initial state
f	Refers to final state
s	Refers to the shell

References

1. J.M. Norbeck, J.W. Heffel, T.D. Durbin, B. Tabbara, J.M. Bowden, and M.C. Montano, *Hydrogen Fuel for Surface Transportation*, SAE International, Warrendale, PA, 1996.
2. A.A. Akunets, N.G. Basov, V.S. Bushuev, V.M. Dorogotovtsev, A.I. Gromov, A.I. Isakov, V.N. Kovylnikov, Y.A. Merkul'ev, A.I. Nikitenko, and S.M. Tolokonnikov, Super-high-strength microballoons for hydrogen storage, *International Hydrogen Energy*, 19(8), 697–700, 1994.
3. G.P. Sutton and O. Biblarz, *Rocket Propulsion Elements*, 7th edn. Wiley & Sons, New York, 2000.
4. N.K. Zhevago and V.I. Glebova, Hydrogen storage in capillary arrays, *Energy Conversion and Management*, 48(5), 1554–1559, 2007.
5. US Department of Energy Hydrogen, Targets for on-board hydrogen storage systems, last accessed on December 20, 2008, http://www.eere.energy.gov/hydrogenandfuelcells/pdfs/freedomcar_tar gets_explanations.pdf.
6. L.M. Das, On-board hydrogen storage systems for automotive application, *International Journal of Hydrogen Energy*, 21(9), 789–800, 1996.
7. S.L. Robinson and J.L. Handrock, Hydrogen storage for vehicular applications: Technology status and key development areas, Sandia National Laboratory Report SAND94-8229-UC-406, 1994.
8. V.A. Yartys and M.V. Lototsky, An overview of hydrogen storage methods, in *Hydrogen Materials Science and Chemistry of Carbon Nanomaterials*, T.N. Veziroglu, S.Y. Zaginaichenko, D.V. Schur, B. Baranowski, A.P. Shpak, V.V. Skorokhod, and A. Kale, eds. Kluwer Academic Publishers, Dordrecht, the Netherlands.

Downloaded by [Laurent Pilon] at 06:37 11 August 2014

9. R.J. Teitel, Hydrogen supply method, US Patent No. 4211537, July 8, 1980.
10. R.J. Teitel, Hydrogen supply system, US Patent No. 4302217, November 24, 1981.
11. M. Herr and J.A. Lercher, Hydrogen storage in microspheres—Final report, ET-TN-03-628, September 9, 2003.
12. A.C. Dillon, K.M. Jones, T.A. Bekkedahl, C.H. Kiang, D.S. Bethune, and M.J. Heben, Storage of hydrogen in single-walled carbon nanotubes, *Nature*, 386(6623), 377–379, 1997.
13. M. Jordá-Beneytoa, F. Suárez-García, D. Lozano-Castellóa, D. Cazorla-Amorós, and A. Linares-Solano, Hydrogen storage on chemically activated carbons and carbon nanomaterials at high pressures, *Carbon*, 45(2), 293–303, 2007.
14. J. Rowsell and O.M. Yaghi, Strategies for hydrogen storage in metal-organic frameworks, *Angewandte Chemie International Edition*, 44, 4670–4679, 2005.
15. B. Sakintuna, F. Lamari-Darkrim, and M. Hirscher, Metal hydride materials for solid hydrogen storage: A review, *International Journal of Hydrogen Energy*, 32(9), 1121–1140, 2007.
16. A. Bouza, C.J. Read, S. Satyapal, and J. Milliken, Annual DOE hydrogen program review hydrogen storage, US Department of Energy, Energy Efficiency and Renewable Energy, Office of Hydrogen, Fuel Cells and Infrastructure Technologies, 2004.
17. S.G. Chalk and J.F. Miller, Key challenges and recent progress in batteries, fuel cells, and hydrogen storage for clean energy systems, *Journal of Power Sources*, 159, 73–80, 2006.
18. R.J. Teitel, Microcavity hydrogen storage final progress report, US Department of Energy and Environment, Report BNL 51439, 1981.
19. L. Yang, B.Z. Jang, and J. Guo, Micro-spheres for storing and delivering hydrogen to fuel cells, in *Proceedings of the International Hydrogen Energy Congress and Exhibition IHEC 2005*, Istanbul, Turkey, July 13–15, 2005, pp. 1–6.
20. K.L. Yan, B.G. Sellars, J. Lo, S. Johar, and M.K. Murthy, Storage of hydrogen by high-pressure microencapsulation in glass, *International of Journal of Hydrogen Energy*, 10, 517–522, 1985.
21. G.A. Banyay, M.M. Shaltout, H. Tiwari, and B.V. Mehta, Polymer and composite foam for hydrogen storage application, *Journal of Materials Processing Technology*, 191(1–3), 102–105, 2007.
22. R.G. Zalosh and S.N. Bajpai, Hydrogen microsphere hazard evaluation, in *Proceedings of the DOE Thermal and Chemical Storage Annual Contractor's Review Meeting*, Tysons Corner, VA, 1981, pp. 211–213.
23. W. Paul and R.V. Jones, Production and separation of small glass spheres, *British Journal of Applied Physics*, 3, 311–314, 1952.
24. E.H. Farnum, J.R. Fries, J.W. Havenhill, M.L. Smith, and D.L. Stoltz, Method for selecting hollow microspheres for use in laser fusion targets, US Patent No. 3997435, December 14, 1976.
25. R.J. Teitel, Development status of microcavity hydrogen storage for automotive applications, in *Proceedings of the DOE Chemical/Hydrogen Energy Systems Contractor Review,* DOE CONF-791127, Reston, VA, 1979, US Department of Energy, Washington, DC.
26. G.D. Rambach, Hydrogen transport and storage in engineered glass microspheres, in *Proceedings of the Sixth Annual US Hydrogen Meeting—Hydrogen Technologies: Moving toward Commercialization*, Alexandria, VA, March 7–9, 1995, National Hydrogen Association, pp. 163–172.
27. G.D. Rambach and C. Hendricks, Hydrogen transport and storage in engineered microspheres, in *Proceedings of the 1996 US DOE Hydrogen Program Review,* NREL/CP-430-21938, Miami, FL, May 1–2, 1996, Vol. 2, pp. 765–772.
28. T. Riis, E.F. Hagen, P.J.S. Vie, and Ø. Ulleberg, Hydrogen production and storage—R&D priorities and gaps, International Energy Agency, 2006, www.iea.org/Textbase/papers/2006/hydrogen.pdf.
29. R.T. Tsugawa, I. Moen, P.E. Roberts, and P.C. Souers, Permeation of helium and hydrogen from glass-microsphere laser targets, *Journal of Applied Physics*, 47(5), 1987–1993, 1976.
30. Y.V.C. Rao, *An Introduction to Thermodynamics*, Universities Press, Hyderabad, India, 2004.
31. J.P. Den Hartog, *Strength of Materials*, Dover Publications, New York, 1961.
32. G.D. Rambach, Hydrogen transport and storage in engineered glass microspheres, in *Proceedings of the US DOE Hydrogen Program Review Meeting, Sandia National Laboratory*, UCR-JC-11708, April 18–21, 1994.

Downloaded by [Laurent Pilon] at 06:37 11 August 2014

33. G.M. Bartenev and D.S. Sanditov, The strength and some mechanical and thermal characteristics of high-strength glasses, *Journal of Non-Crystalline Solids*, 48(2–3), 405–421, 1982.
34. D.K. Kohli, R.K. Khardekar, R. Singh, and P.K. Gupta, Glass micro-container based hydrogen storage scheme, *International of Hydrogen Energy*, 33(1), 417–422, 2008.
35. D. Duret and A. Saudin, Microspheres for on-board hydrogen storage, *International of Journal of Hydrogen Energy*, 19, 757–764, 1994.
36. H. Kunieda, Classical buckling load of spherical domes under uniform pressure, *Journal of Engineering Mechanics*, 118(8), 1513–1525, 1992.
37. N.F. Morris, Shell stability: The long road from theory to practice, *Engineering Structures*, 18(10), 801–806, 1996.
38. W. Wunderlich and U. Albertin, Buckling behaviour of imperfect spherical shells, *International Journal of Non-Linear Mechanics*, 37(4–5), 589–604, 2002.
39. M. Deml and W. Wunderlich, Direct evaluation of the 'worst' imperfection shape in shell buckling, *Computer Methods in Applied Mechanics and Engineering*, 149(1–4), 201–222, 1997.
40. J.E. Shelby, *Handbook of Gas Diffusion in Solids and Melts*, ASM International, Materials Park, OH, 1996.
41. F.J. Norton, Helium diffusion through glass, *Journal of the American Ceramic Society*, 36(3), 90–96, 1953.
42. F.J. Norton, Permeation of gases through solids, *Journal of Applied Physics*, 28(1), 34–39, 1957.
43. H.J. Frost and R. Raj, Limiting densities for dense random packing of spheres, *Journal of the American Ceramic Society*, 65(2), C-19–C-21, 1982.
44. Z. Pientka, P. Pokorný, and K. Belafi-Bako, Closed-cell polymeric foam for hydrogen separation and storage, *Journal of Membrane Science*, 304(1–2), 82–87, 2007.
45. L. Pilon, A.G. Fedorov, and R. Viskanta, Gas diffusion in closed-cell foams, *Journal of Cellular Plastics*, 36, 451–474, 2000.
46. D.N. Sutherland, Random packing of circles in a plane, *Journal of Colloid and Interface Science*, 60(1), 96–102, 1977.
47. N.P. Bansal and R.H. Doremus, *Handbook of Glass Properties*, Academic Press, Inc., Orlando, FL, 1986.
48. G.W. McLellan and E.B. Shand, *Glass Engineering Handbook*, 3rd edn. Mc Graw Hill, New York, 1984.
49. R.H. Doremus, *Glass Science*, 2nd edn. John Wiley & Sons, New York, 1994.
50. H. Rawson, *Properties and Applications of Glass*, Elsevier, New York 1980.
51. W.D. Johnston and A.J. Chelko, Reduction of ions in glass by hydrogen, *Journal of American Ceramics Society*, 53(6), 295–301, 1970.
52. J.E. Shelby and J. Vitko Jr., Hydrogen transport in a machinable glass-ceramic, *Journal of Non-Crystalline Solids*, 45, 83–92, 1981.
53. P.C. Souers, I. Moen, R.O. Lindhal, and R.T. Tsugawa, Permeation eccentricities of He, Ne, and D-T from soda-lime glass microbubbles, *Journal of the American Ceramic Society*, 61(1–2), 42–46, 1978.
54. R.H. Doremus, Pre-exponential factor of temperature in the diffusion equation, *Journal of Chemical Physics*, 34(6), 2186–2187, 1961.
55. V.O. Altemose, Helium diffusion through glass, *Journal of Applied Physics*, 32(7), 1309–1316, 1961.
56. R.W. Lee, R.C. Frank, and D.E. Swets, Diffusion of hydrogen and deuterium in fused quartz, *The Journal of Chemical Physics*, 36(4), 1062–1071, 1962.
57. R.W. Lee, Diffusion of hydrogen in natural and synthetic fused quartz, *The Journal of Chemical Physics*, 38(2), 448–455, 1963.
58. H.M. Laska, R.H. Doremus, and P.J. Jorgensen, Permeation, diffusion, and solubility of deuterium in pyrex glass, *Journal of Chemical Physics*, 50(1), 135–137, 1969.
59. J.L. Barton and M. Morain, Hydrogen diffusion in silicate glass, *Journal of Non-Crystalline Solids*, 3, 115–126, 1970.
60. J.E. Shelby, Helium, deuterium, and neon migration in a common borosilicate glass, *Journal of Applied Physics*, 45(5), 2146–2149, 1974.

Downloaded by [Laurent Pilon] at 06:37 11 August 2014

61. N. Kurita, N. Fukatsu, H. Otsuka, and T. Ohashi, Measurements of hydrogen permeation through fused silica and borosilicated glass by electrochemical pumping using oxide protonic conductor, *Solid State Ionics*, 146, 101–111, 2002.
62. J.E. Shelby and B.E. Kenyon, Glass membrane for controlled diffusion of gases, US Patent No. 6231642 B1, May 15, 2001.
63. B.E. Kenyon, Gas solubility and accelerated diffusion in glasses and melts, Master's thesis, Alfred University, Alfred, NY, 1998.
64. D.B. Rapp and J.E. Shelby, Photo-induced hydrogen outgassing of glass, *Journal of Non-Crystalline Solids*, 349, 254–259, 2004.
65. D.B. Rapp, Photo-induced hydrogen outgassing of glass, PhD thesis, Alfred University, Alfred, NY, 2004.
66. R.K. Brow and M.L. Schmitt, A survey of energy and environmental applications of glass, *Journal of the European Ceramic Society*, 29(7), 1193–1201, 2009.
67. R. Kitamura and L. Pilon, Radiative heat transfer in enhanced hydrogen outgassing of glass, *International Journal of Hydrogen Energy*, 34(16), 6690–6704, 2009.
68. R. Kitamura, L. Pilon, and M. Jonasz, Optical constants of silica glass from extreme ultraviolet to far infrared at near room temperature, *Applied Optics*, 46(33), 8118–8133, 2007.
69. R. Viskanta and J. Lim, Transient cooling of a cylindrical glass gob, *Journal of Quantitative Spectroscopy and Radiation Transfer*, 73, 481–490, 2002.
70. D. De Sousa Meneses, G. Gruener, M. Malki, and P. Echegut, Causal Voigt profile for modeling reflectivity spectra of glasses, *Journal of Non-Crystalline Solids*, 351, 124–129, 2005.
71. J.E. Shelby and J. Vitko Jr., The reduction of iron in soda-lime-silicate glasses by reaction with hydrogen, *Journal of Non-Crystalline Solids*, 53, 155–163, 1982.
72. S.P. Faile and D.M. Roy, Dissolution of hydrogen in fused quartz, *Journal of American Ceramics Society*, 54(10), 533–534, 1971.
73. I. Fanderlik, *Glass Science and Technology, Vol. 5: Optical Properties of Glass*, Elsevier Science, New York, 1983.
74. W. Schotte, Thermal conductivity of packed beds, *AIChE Journal*, 6(1), 63–67, 1960.
75. J.C. Chen and S.W. Churchill, Radiant heat transfer in packed beds, *AIChE Journal*, 8, 35–41, 1963.
76. M.Q. Brewster and C.L. Tien, Radiative transfer in packed fluidized beds: Dependent versus independent scattering, *ASME Journal of Heat Transfer*, 104, 573–579, 1982.
77. K. Kamiuto, Correlated radiative transfer in packed-sphere systems, *Journal of Quantitative Spectroscopy and Radiative Transfer*, 43, 39–43, 1990.
78. K. Kamiuto, M. Iwamoto, M. Sato, and T. Nishimura, Radiation-extinction coefficients of packed-sphere systems, *Journal of Quantitative Spectroscopy and Radiative Transfer*, 45, 93–96, 1991.
79. K. Kamiuto, Analytical expression for total effective thermal conductivities of packed beds, *Journal of Nuclear Science and Technology*, 28(12), 1153–1156, 1991.
80. B.P. Singh and M. Kaviany, Independent theory versus direct simulation of radiative heat transfer in packed beds, *International Journal of Heat and Mass Transfer*, 34, 2869–2882, 1991.
81. B.P. Singh and M. Kaviany, Modelling radiative heat transfer in packed beds, *International Journal of Heat and Mass Transfer*, 35, 1397–1405, 1992.
82. K. Kamiuto, Radiative properties of packed-sphere systems estimated by the extended emerging-intensity fitting method, *Journal of Quantitative Spectroscopy and Radiative Transfer*, 47, 257–261, 1992.
83. K. Kamiuto, Combined conduction and correlated-radiation heat transfer in packed beds, *Journal of Thermophysics and Heat Transfer*, 7(3), 496–501, 1993.
84. M. Kaviany and B.P. Singh, Radiative heat transfer in porous media, *Advances in Heat Transfer*, 23(23), 133–186, 1993.
85. K. Nasr, R. Viskanta, and S. Ramadhyani, An experimental evaluation of the effective thermal conductivities of packed beds at high temperatures, *ASME Journal of Heat Transfer*, 116(4), 829–837, 1994.

Downloaded by [Laurent Pilon] at 06:37 11 August 2014

86. U. Bossel, Does a hydrogen economy make sense? *Proceedings of the IEEE*, 94(10), 1826–1837, 2006.
87. S.L. Robinson and J.J. Iannucci, Technologies and economics of small-scale hydrogen storage, Sandia National Laboratory Report SAND-79–8646, 1979.
88. B.A. Proctor, Strengths of acid-etched glass rods, *Nature*, 187, 492–493, 1960.
89. A.S. Geleil, M.M. Hall, and J.E. Shelby, Hollow glass microspheres for use in radiation shielding, *Journal of Non-Crystalline Solids*, 352(6–7), 620–625, 2006.
90. C.D. Hendricks, Glass spheres, in *Materials Handbook, Ceramics and Glasses,* Vol. 4, S.J. Schneider Jr., ed. ASM International, Materials Park, OH.
91. J. Bertling, J. Blömer, and R. Kümmel, Hollow microspheres, *Chemical Engineering Technology*, 27(8), 829–837, 2004.
92. V.V. Budov, Hollow glass microspheres. use, properties, and technology (review), *Glass and Ceramics*, 51(7–8), 230–235, 1994.
93. E.F. Medvedev, Use of structural criteria for calculating oxide glass compositions for hydrogen microcontainers (a review), *Glass and Ceramics*, 63(7–8), 222–226, 2006.
94. F. Veatch and R.W. Burhans, Process of producing hollow particles and resulting product, US Patent 2797201, June 25, 1957.
95. F. Veatch, H.E. Alford, and R.C. Croft, Hollow glass particles and method of producing the same, US Patent No. 2978340, April 4, 1961.
96. F. Veatch, H.E. Alford, and R.C. croft, Apparatus for producing hollow glass particles, US Patent No. 3129086, April 14, 1964.
97. W.R. Beck and D.L. O'Brien, Glass bubbles prepared by reheating solid glass particles, US Patent No. 3365315, January 23, 1968.
98. H.E. Alford and F. Veatch, Microsphere glass agglomerates and method for making them, US Patent No. 3458332, July 29, 1969.
99. C.D. Hendricks, Method for producing small hollow spheres, US Patent No. 4133854, January 9, 1979.
100. A. Rosencwaig, J.C. Koo, and J.L. Dressler, Method for producing small hollow spheres, US Patent No. 4257799, March 24, 1981.
101. P.A. Howell, Glass bubbles of increased collapse strength, US Patent No. 4391646, July 5, 1983.
102. P. Garnier, D. Abriou, and M. Coquillon, Process for producing glass microspheres, US Patent No. 4661137, April 28, 1987.
103. H.J. Marshall, Glass microbubbles, US Patent No. 4767726, August 30, 1988.
104. P. Garnier, D. Abriou, and J.-J. Gaudiot, Production of glass microspheres, US Patent No. 4778502, October 18, 1988.
105. R.W.J. Lencki, R.J. Neufeld, and T. Spinney, Method of producing microspheres, US Patent No. 4822534, April 18, 1989.
106. K.E. Goetz, J.A. Hagarman, and J.P. Giovene Jr., Hollow glass spheres, US Patent No. 4983550, January 8, 1991.
107. J. Block, N.J. Tessier, and A.J. Colageo, Method of making small hollow glass spheres, US Patent No. 5069702, December 3, 1991.
108. R.W. Rice A.J. Colageo J. Block, J.W. Lau, Method for making low sodium hollow glass microspheres, US Patent No. 5176732, January 5, 1993.
109. P. Garnier, D. Abriou, and J.-J. Gaudiot, Method for selecting hollow microspheres for use in laser fusion targets, US Patent No. 5256180, October 26, 1993.
110. S. Kawachi and Y. Sato, Glass composition for glass bubbles with increased compressive strength, US Patent No. 5292690, March 8, 1994.
111. E.V. Sokol, N.V. Maksimova, N.I. Volkova, E.N. Nigmatulina, and A.E. Frenkel, Hollow silicate microspheres from fly ashes of the Chelyabinsk brown coals (South Urals, Russia), *Fuel Processing Technology*, 67(1), 35–52, 2000.
112. L.K. Heung, R.F. Schumacher, and G.G. Wicks, Hollow porous-wall glass microspheres for hydrogen storage, Patent Application No. US 2006/0059953 (October 21, 2005) and International Application No. PCT/US2006/040525 (October 17, 2006).

Downloaded by [Laurent Pilon] at 06:37 11 August 2014

113. G.G. Wicks, L.K. Heung, and R.F. Schumacher, Microspheres and microworlds, *ACerS Bulletin*, 23–28, June 2008.
114. J.R. Fisher and M.D. Rigterink, Formation of expanded silica spheres, US Patent No. 2883347, April 21, 1959.
115. V.V. Budov and V.Y. Stetsenko, Choice of glass composition for producing hollow microspheres, *Glass and Ceramics*, 45(8), 289–291, 1988.
116. V.V. Budov, Physicochemical processes in producing hollow glass microspheres, *Glass and Ceramics*, 47(3), 77–79, 1990.
117. I. Bica, Formation of glass microspheres with rotating electrical arc, *Materials Science and Engineering B*, 77, 210–212, 2000.
118. P.D. Law, Method and apparatus for production of glass beads by use of a rotating wheel, US Patent No. 3310391, March 21, 1967.
119. E.M. Guyer and J.E. Nitsche, Method and apparatus for manufacturing glass beads, US Patent No. 3313608, April 11, 1967.
120. R.L. Downs and W.J. Miller, Hollow microspheres of silica glass and method of manufacture, US Patent No. 4336338, June 22, 1982.
121. C.D. Hendricks, A. Rosencwaig, R.L. Woerner, J.C. Koo, J.L. Dressler, J.W. Sherohman, S.L. Weinland, and M. Jeffries, Fabrication of glass sphere laser fusion targets, *Journal of Nuclear Materials*, 85–86(1), 107–111, 1979.
122. T.P. O'Holleran, R.L. Nolen, R.L. Downs, D.A. Steinman, and R.L. Crawley, Summary abstract: Shells from compacted powders, *Journal of Vacuum Science and Technology*, 18(3), 1242–1243, 1981.
123. M.L. Schmitt, J.E. Shelby, and M.M. Hall, Preparation of hollow glass microspheres from sol-gel derived glass for application in hydrogen gas storage, *Journal of Non-Crystalline Solids*, 352(6–7), 626–631, 2006.
124. A. Rosencwaig, J.L. Dressler, J.C. Koo, and C.D. Hendricks, Laser fusion hollow glass microspheres by the liquid-droplet method, Lawrence Livermore Laboratory Report UCRL-81421, June 5, 1978.
125. C.D. Hendricks, Fuel pellets and optical systems for inertially confined fusion, *Journal of Nuclear Materials*, 85–86(1), 79–86, 1979.
126. J. Koo, J. Dressler, and C. Hendricks, Low pressure gas filling of laser fusion microspheres, *Journal of Nuclear Materials*, 85–86(1), 113–115, 1979.
127. J.Y. Dinga and D.E. Day, Preparation of silica glass microspheres by sol-gel processing, *Journal of Materials Research*, 6(1), 168–174, 1991.
128. F. Caruso, R.A. Caruso, and H. Möhwald, Nanoengineering of inorganic and hybrid hollow spheres by colloidal templating, *Science*, 282(5391), 1111–1114, 1998.
129. B. Peng, M. Chen, S. Zhou, L. Wu, and X. Ma, Fabrication of hollow silica spheres using droplet templates derived from a miniemulsion technique, *Journal of Colloid and Interface Science*, 321(1), 67–73, 2008.
130. K.K. Kim, K.Y. Jang, and R.S. Upadhye, Hollow silica spheres of controlled size and porosity by sol-gel processing, *Journal of the American Ceramic Society*, 74(8), 1987–1992, 1991.
131. K.Y. Jang and K. Kim, Evaluation of sol-gel processing as a method for fabricating spherical-shell silica aerogel inertial confinement fusion targets, *Journal of Vacuum Science & Technology A*, 10, 1152–1157, 1992.
132. B. Tan and S.E. Rankin, Dual latex/surfactant templating of hollow spherical silica particles with ordered mesoporous shells, *Langmuir*, 21(18), 8180–8187, 2005.
133. S. Zhang, L. Xu, H. Liu, Y. Zhao, Y. Zhang, Q. Wang, Z. Yu, and Z. Liu, A dual template method for synthesizing hollow silica spheres with mesoporous shells, *Materials Letters*, 63(2), 258–259, 2009.
134. Y.-Q. Yeh, B.-C. Chen, H.-P. Lin, and C.-Y. Tang, Synthesis of hollow silica spheres with mesostructured shell using cationic-anionic-neutral block copolymer ternary surfactants, *Langmuir*, 22(1), 6–9, 2006.

Downloaded by [Laurent Pilon] at 06:37 11 August 2014

135. N. Kato, T. Ishii, and S. Koumoto, Synthesis of monodisperse mesoporous silica hollow microcapsules and their release of loaded materials, *Langmuir*, 26(17), 14334–14344, 2010.
136. S. Schacht, Q. Huo, I.G. Voigt-Martin, G.D. Stucky, and F. Schth, Oil-water interface templating of mesoporous macroscale structures, *Science*, 273(5276), 768–771, 1996.
137. Z. Teng, Y. Han, J. Li, F. Yan, and W. Yang, Preparation of hollow mesoporous silica spheres by a sol-gel/emulsion approach, *Microporous and Mesoporous Materials*, 127(1–2), 67–72, 2010.
138. B.A. Proctor, I. Whitney, and J.W. Johnson, The strength of fused silica, *Proceedings of the Royal Society of London. Series A, Mathematical and Physical Sciences*, 297(1451), 534–557, 1967.
139. C.S. Chamberlain, G.F. Vesley, P.G. Zimmerman, and J.W. McAllister, Coated glass microbubbles and article incorporating them, US Patent No. 4618525, October 21, 1986.
140. Zhang, Q., Wu, M., and Zhao, W., Electroless nickel plating on hollow glass microspheres, *Surface and Coatings Technology*, 192(2–3), 213–219, 2005.
141. K.H. Moh, Glass and glass-ceramic bubbles having an aluminum nitride coating, US Patent No. 5691059, November 25, 1997.
142. M.E. Holman, Gel-coated microcapsules, US Patent No. 6099894, August 8, 2000.
143. A.G. Baker and A.J. Baker, Process for producing hollow, bilayered silicate microspheres, US Patent No. 4549892, October 29, 1985.
144. Q. Sun, P.J. Kooyman, J.G. Grossmann, P.H.H. Bomans, P.M. Frederik, P.C.M.M. Magusin, T.P.M. Beelen, R.A. van Santen, and N.A.J.M. Sommerdijk, The formation of well-defined hollow silica spheres with multilamellar shell structure, *Advances in Materials*, 15, 1097–1100, 2003.
145. M. Okubo and H. Minami, Control of hollow size of micron-sized monodispersed polymer particles having a hollow structure, *Colloid & Polymer Science*, 274(5), 433–438, 1996.
146. W. Schmidt and G. Roessling, Novel manufacturing process of hollow polymer microspheres, *Chemical Engineering Science*, 61(15), 4973–4981, 2006.
147. G. Crotts and T.G. Park, Preparation of porous and nonporous biodegradable polymeric hollow microspheres, *Journal of Controlled Release*, 35, 91–105, 1995.
148. T. Brandau, Preparation of monodisperse controlled release microcapsules, *International Journal of Pharmaceutics*, 242, 179–184, 2002.
149. J.A. Burgman and L.L. Margason, Method and apparatus for forming hollow glass fibers, US Patent No. 3268313, August 23, 1966.
150. T.H. Jensen, Hollow glass fiber bushing, method of making hollow fibers and the hollow glass fibers made by that method, US Patent No. 4758259, July 19, 1988.
151. T. Maruyama, H. Matsumoto, and Y. Miyake, Glass capillary tube and method for its production, US Patent No. 4882209, November 21, 1989.
152. P. Muthukumar, M.P. Maiya, and S.S. Murthy, Performance tests on a thermally operated hydrogen compressor, *International Journal of Hydrogen Energy*, 33(1), 463–469, 2008.
153. P. Muthukumar, M.P. Maiya, and S.S. Murthy, Parametric studies on a metal hydride based single stage hydrogen compressor, *International Journal of Hydrogen Energy*, 27(10), 1083–1092, 2002.
154. E.W. Lemmon, M.L. Huber, and M.O. McLinden, NIST reference fluid thermodynamic and transport properties database (REFPROP): Version 8.0, National Institute of Standards and Technology, Boulder, CO, 2007, http://www.nist.gov/srd/nist23.htm.
155. N. Sahba and T.J. Rockett, Infrared absorption coefficients of silica glasses, *Journal of the American Ceramic Society*, 75(1), 209–212, 1992.

Downloaded by [Laurent Pilon] at 06:37 11 August 2014

Downloaded by [Laurent Pilon] at 06:37 11 August 2014